

Fermionic equations of motion in strongly-correlated media: applications to the nuclear many-body problem

Elena Litvinova^{1,2,3}

¹*Department of Physics, Western Michigan University, Kalamazoo, MI 49008, USA*

²*Facility for Rare Isotope Beams, Michigan State University, East Lansing, MI 48824, USA*

³*GANIL, CEA/DRF-CNRS/IN2P3, F-14076 Caen, France*

(Dated: December 25, 2024)

These notes summarise the lectures given at the International School of Physics 'Enrico Fermi' in Summer 2024 in Varenna (Italy) about the strongly coupled quantum many-body theory and its applications to nuclear structure. The lectures present a rather short overview of the subject with an emphasis on the analytical aspects of the nuclear many-body problem, aiming at a deep understanding of the complexity of strongly coupled nucleonic states and emergent collective phenomena. The major pedagogical focus is recognizing how all the models describing nuclear dynamics follow from a unified model-independent framework formulated in the universal language of quantum field theory. In particular, connections between the classes of ab initio, density functional theory, and beyond mean-field approaches are made accessible. Approximations of varying complexity are discussed in applications to excited states of medium-heavy nuclei.

I. INTRODUCTION

The nuclear many-body problem underlies nearly all the physics frontiers and applications, from fundamentals to technologies. Accurate quantitative predictions of nuclear properties have remained challenging for decades. Driven by newly emerging intellectual and computational capabilities, this field has shown substantial progress over the years; however, reliable computation of atomic nuclei still calls for further developments in theory and numerical implementations. One of the most powerful tools to study strongly correlated fermionic many-body systems is the Green function (GF) method. Various Green functions, or propagators, belonging to a larger class of correlation functions (CFs), form a common theoretical background across the energy scales. The GFs can be straightforwardly related to most accessible observables of the fermionic systems [1–7]: the single-particle propagators are linked to the energies of odd-particle systems and spectroscopic factors which can be extracted from transfer or knock-out reactions. The two-fermion particle-hole propagators quantify the response of the system to external probes, such as the electromagnetic, strong, or weak ones in the case of atomic nuclei. Superfluidity can be efficiently described by two-particle in-medium pair propagators and probed by pair transfer, while the residues of those propagators can be linked to the pairing gaps in the low-energy spectra [8, 9].

The low-rank propagators are mostly relevant to the observed phenomena, however, higher-rank CFs appear as part of the general theory in the dynamical kernels of the equations of motion (EOMs), characterizing their lower-rank counterparts [5–7, 10]. Generally, the dynamical kernels are the source of coupling between EOMs for propagators of all ranks relevant to the given system into a hierarchy, which can be decoupled by making certain approximations. The higher-rank propagators correspond to correlated multi-fermion configurations embed-

ded in the medium and quantify the dynamical effects of long-range correlations. In these lectures, we will see that in the intermediate and strong coupling regimes, the higher-rank GFs encode emergent collective effects. At intermediate coupling associated with atomic nuclei, the emergent degrees of freedom can establish new order parameters and promote the connections between the degrees of freedom across the energy scales.

Most often, textbook formulation of the GF method operates non-symmetric dynamical kernels [11], which are subsequently expanded in perturbation series or factorization in terms of single-fermion GFs. The particular advantages of the symmetric forms of the dynamical kernels were pointed out and elaborated by Peter Schuck and coauthors [12–14]. Considering symmetric kernels is especially insightful for finding advanced solutions to the quantum many-body problem via factorizations retaining formally exact two-fermion CFs, with applications ranging from particle physics [15, 16] to nuclear structure [17, 18] to quantum chemistry and condensed matter physics [19–24]. Interestingly, beyond-mean-field (BMF) approaches actively employed in calculations for medium-heavy nuclei based on effective interactions can be related to the Hamiltonians operating bare fermionic interactions [17, 24–27]. The BMF approaches that account for emergent collective effects of the nuclear medium are of particular interest for medium-heavy nuclei with pronounced collectivity. They can be continuously derived ab initio, i.e., employing only the bare interaction, by retaining the correlated pairs of fermionic quasiparticles in the dynamical kernels of the EOMs for the propagators related to the required observables. These correlated pairs are known as phonons, which emerge as mediators of the dynamical in-medium interaction between fermions and exist on shells as collective excitations. The interaction, or coupling, between quasiparticles and phonons is the central part of the nuclear field theory (NFT) elaborated by the Copenhagen-Milano school, particularly Ricardo Broglia [28–33], NFT variants based on the Migdal's the-

ory [34–36] and the quasiparticle-phonon model (QPM) of V.G. Soloviev and collaborators [37, 38].

By definition of the ab initio EOM, the static and dynamical kernels of the two-quasiparticle CFs play the role of the in-medium interaction between the fermions. The former kernel is responsible for the short-range correlations, while the latter governs the long-range ones. As will be discussed in detail below, the short-range kernel contains contractions of the bare fermionic interaction with two-body densities, and the long-range one accommodates the fully correlated four-fermion CF. The presence of these CFs in the interaction kernels makes the EOM non-linear and the exact solution intractable, but even for the approximations with reasonably factorized dynamical kernels, entering the self-consistent cycle of the non-linear EOM requires some educated guess about the static kernel. While the fully consistent ab initio calculations are not yet available, in practical applications, the static kernel can be well approximated by effective interactions derived, e.g., from the density functional theories (DFTs). The procedure to correct for inaccuracies of this approximation by subtraction of the Pauli-Villars type [39] recovering the static limit of the full kernel allows one to avoid inconsistencies associated with this replacement in the self-consistent implementations of the response theory [17, 40–45].

As the majority of atomic nuclei and many other fermionic systems are essentially superfluid, an EOM for the single-quasiparticle propagator has been formulated for the superfluid case in Ref. [46] continuing the research line of the preceding work [47–60]. It was shown in Ref. [46], in particular, how pairing correlations beyond the Hartree-Fock-Bogolyubov (HFB) approximation are integrated into ab-initio theory with the dynamical kernel keeping the two-fermion CFs responsible for the leading effects of emergent collectivity. Transforming the exact single-fermion EOM to the basis of the Bogolyubov quasiparticles has allowed for consistent unification of the normal and pairing phonon modes and considerable compactification of the superfluid Dyson equation in a general framework. This enables for remarkably more efficient handling of the dynamical kernels beyond the HFB approach than those of the Gor'kov Green functions and a link of the quasiparticle-vibration coupling (qPVC) vertices to the variations of the Bogolyubov quasiparticle Hamiltonian. Ref. [61] elaborated on the EOM for the response function, which has been worked out in the basis of Bogolyubov quasiparticles from the beginning, leading to a comprehensive ab initio response theory for superfluid fermionic systems. The developed formalism allows for analyzing dynamical kernels with varying correlation content and generating the known phenomenological approaches, such as the second RPA (SRPA), NFT, and its extensions, in certain limits.

The formal part of these lecture notes is focused on the EOMs for the two-point fermionic propagators in strongly correlated media with an emphasis on the dynamical interaction kernels. Starting with the many-

body Hamiltonian confined by a two-body interaction between two fermions in the vacuum, it is shown by continuous derivation how the EOMs for the two-point in-medium fermionic propagators acquire the Dyson form. I elaborate specifically on the one-fermion and two-fermion CFs related to the single-particle observables and response to external probes of various natures. Before taking any approximation, the interaction kernels of the respective EOMs decompose into static and dynamic (time-dependent) contributions. The latter translates to the energy-dependent, and the former maps to the energy-independent terms in the energy domain. Furthermore, it is argued that the static kernels are not well-known due to the difficulty of their accurate determination, which justifies the efficiency of applying the concept of effective interaction compared to fully ab initio approaches operating exclusively on bare interactions. I dwell particularly on the dynamic terms, which generate long-range correlations while giving feedback on their short-range static counterparts. The origin, forms, and various approximations for the dynamical kernels of one-fermion and two-fermion propagators, most relevant in the intermediate-coupling regime, are discussed.

Special emphasis is put on the aspects elaborated and inspired by the scientific work of Ricardo Broglia. This pertains to dynamical kernels, where the many-body problem is truncated on the two-body level, i.e., variants of the qPVC kernels, which have been widely explored by NFT over decades [31–33, 50, 51, 62–67]. These approximations are found to be very efficient for the applications to the regimes of intermediate coupling as they allow for a reasonable compromise between accuracy and feasibility. The latter is possible by making use of modern effective interactions, and the former is enabled by the qPVC as the leading approximation to emergent collectivity. Recent numerical implementations for the nuclear response with the self-consistent relativistic qPVC are discussed in light of their relevance to exotic nuclear phenomena and astrophysical applications.

I discuss these recent developments and their implementations for nuclear structure calculations, where the dynamical kernels accounting for emergent collectivity play an important role. In the nuclear response theory for medium-heavy nuclei, it is of prime importance that such kernels introduce correlations beyond the simplistic random phase approximation (RPA) and include higher (correlated) two-particle-two-hole ($2p2h$) [41, 42, 44, 65, 66, 68–71] configuration complexity. After decades of exploring such approximations, it has become evident that, although the latter configuration complexity is necessary to improve the description of nuclear excited states, they are still insufficient for reproducing spectral richness and spectroscopically accurate results.

A path to higher configuration complexity was set by the QPM of V.G. Soloviev and collaborators [37, 72, 73]. QPM is formulated in the basis of phonons evaluated by the quasiparticle random phase approximation (QRPA), i.e., correlated two-quasiparticle pairs, and admits com-

plex wave functions in the form of multiphonon configurations [74–79]. QPM implementations were advanced to the $3p3h$, or three-phonon, configuration complexity for medium-heavy nuclei in model spaces limited by low energy and showed success [80–84]. Although these implementations exist only in non-selfconsistent frameworks and require adjustments of the interaction parameters to data for each multipole, they show unambiguously that to reproduce the richness of the observed spectra, at least $3p3h$ configuration complexity should be included in the theory. Therefore, considerable effort was dedicated to including such configurations, which has become possible recently in larger model spaces up to high energy (25–30 MeV) [17, 18, 85, 86] with the current computational capabilities. An overarching goal is developing a predictive approach demonstrating consistent performance of spectroscopic accuracy across the nuclear chart. The effort toward such an approach includes advancements in its two major building blocks: (i) the nucleon-nucleon (NN) interactions and (ii) the quantum many-body methods, which are deeply interrelated. In these notes, I focus on the latter aspect and accurate modeling of the in-medium fermionic dynamics using NN interactions as an input to the theory. The formalism section will closely follow that of Ref. [18] complemented by extended methodical recommendations.

II. FERMIONIC PROPAGATORS IN A CORRELATED MEDIUM

A. Definitions and microscopic input to the many-body theory

The starting point for the many-body theory can be the system's Lagrangian or, alternatively, its Hamiltonian. The Hamiltonian formulation is especially convenient for dynamical theory, which tracks explicit time dependence. The many-body Hamiltonian in the field-theoretical representation generally reads

$$H = H^{(1)} + V^{(2)} + W^{(3)} + \dots, \quad (1)$$

where the operator $H^{(1)}$ describes the one-body contribution:

$$H^{(1)} = \sum_{12} t_{12} \psi_1^\dagger \psi_2 + \sum_{12} v_{12}^{(MF)} \psi_1^\dagger \psi_2 \equiv \sum_{12} h_{12} \psi_1^\dagger \psi_2 \quad (2)$$

with matrix elements h_{12} combining the kinetic energy t and the mean-field $v^{(MF)}$ part of the interaction, and ψ_1, ψ_1^\dagger are destruction and creation fermionic field operators in some basis completely characterized by the number indices. In this work, we focus on the EOMs for fermionic fields, while bosonic fields will mediate the interaction between fermions. The latter is quantified by the interaction operator $V^{(2)}$ between two-fermions:

$$V^{(2)} = \frac{1}{4} \sum_{1234} \bar{v}_{1234} \psi_1^\dagger \psi_2^\dagger \psi_4 \psi_3, \quad (3)$$

where the antisymmetrized matrix elements $\bar{v}_{1234} = v_{1234} - v_{1243}$ express the meson exchange either explicitly or in some form of effective field theory. $W^{(3)}$ formally stands for the three-body forces, which are neglected in the presented formalism because, eventually, the numerical implementation of the theory discussed in Section III is performed in a relativistic framework. We will not use explicitly covariant notations in these lectures; however, bear in mind that the relativistic field-theoretical Hamiltonian of interacting nucleons is defined by the terms of essentially the same form as $H^{(1)}$ and $V^{(2)}$ [87, 88]. Because of that, the general structure of the fermionic EOMs defined by the fermionic field operator composition of H remains the same. Our expressions for the one-fermion EOM with a non-symmetric form of the dynamical kernel can be compared, for instance, with those of Refs. [89, 90]. Neglecting $W^{(3)}$ is justified by the fact that the role of three-body forces in a relativistic theory is considerably smaller than in a non-relativistic one. Whether the relativistic three-body forces should be included in the description of nuclear systems is not completely clear. Quantitative studies of this subject were reported only for the few-body systems [91, 92]. We argue that an adequate non-perturbative description of in-medium fermionic propagators should generate the three- and higher-body forces identifiable as in Ref. [92] and thus must realistically include their contributions, at least in medium-mass and heavy nuclei.

The fermionic fields obey the usual anticommutation relations

$$\begin{aligned} [\psi_1, \psi_{1'}^\dagger]_+ &\equiv \psi_1 \psi_{1'}^\dagger + \psi_{1'}^\dagger \psi_1 = \delta_{11'}, \\ [\psi_1, \psi_{1'}]_+ &= [\psi_1^\dagger, \psi_{1'}^\dagger]_+ = 0, \end{aligned} \quad (4)$$

and undergo time evolution in the Heisenberg picture:

$$\psi(1) = e^{iHt_1} \psi_1 e^{-iHt_1}, \quad \psi^\dagger(1) = e^{iHt_1} \psi_1^\dagger e^{-iHt_1}. \quad (5)$$

The CF of two fermionic field operators introduces the one-fermion in-medium propagator or its real-time Green function:

$$G(1, 1') \equiv G_{11'}(t - t') = -i \langle T \psi(1) \psi^\dagger(1') \rangle, \quad (6)$$

via the chronological ordering operator T and the averaging $\langle \dots \rangle$ over the many-body ground state of the system containing N interacting fermions (e.g., nucleons). The correlation function $G_{11'}(t - t')$ describes the probability amplitude of a single fermion to travel through a medium of identical interacting fermions.

Basis choice is essential as it can simplify applications of formalism considerably. On the contrary, an inconveniently chosen basis can greatly complicate calculations. One common choice in the EOM method is the basis of fermionic states $\{1\}$ diagonalizing simultaneously the one-body part of the Hamiltonian $H^{(1)}$: $h_{12} = \delta_{12} \varepsilon_1$ and the corresponding density matrix. As follows from Eq. (6), the propagator $G_{11'}(t - t')$ is time translational invariant, i.e., depends explicitly on the time difference

$\tau = t - t'$. Thus, its Fourier image is a function of a single energy (frequency). Indeed, inserting the operator $\mathbb{1} = \sum_n |n\rangle\langle n|$ with the complete set of the many-body states $|n\rangle$, one arrives at the spectral expansion, or Källén - Lehmann representation [93, 94]:

$$G_{11'}(\varepsilon) = \sum_n \frac{\eta_1^n \eta_{1'}^{n*}}{\varepsilon - (E_n^{(N+1)} - E_0^{(N)}) + i\delta} + \sum_m \frac{\chi_1^m \chi_{1'}^{m*}}{\varepsilon + (E_m^{(N-1)} - E_0^{(N)}) - i\delta}. \quad (7)$$

Thus, in the energy domain, the propagator (6) is a series of simple poles with factorized residues. This is the common feature of propagators in quantum field theory (QFT), expressing its locality and unitarity. The poles are the formally exact energies $E_n^{(N+1)} - E_0^{(N)}$ and $-(E_m^{(N-1)} - E_0^{(N)})$ of the $(N+1)$ -particle and $(N-1)$ -particle systems, respectively, above the ground state of the reference N -particle system. The corresponding residues are the matrix elements

$$\eta_1^n = \langle 0^{(N)} | \psi_1 | n^{(N+1)} \rangle, \quad \chi_1^m = \langle m^{(N-1)} | \psi_1 | 0^{(N)} \rangle \quad (8)$$

of the fermionic operators between the ground state $|0^{(N)}\rangle$ of the N -particle system and states $|n^{(N+1)}\rangle$ and $|m^{(N-1)}\rangle$ of the neighboring systems. The latter are the overlaps of the single-particle (single-hole) configurations $\{1\}$ on top of the ground state $|0^{(N)}\rangle$ in the n -th (m -th) state of the $(N+1)$ -particle ($(N-1)$ -particle) systems. The residues in Eq. (7) are thus associated with the (generally fractional) occupancies of the correlated fermionic states.

The EOM for the propagator $G_{11'}(t - t')$, introduced and discussed in the next subsection, connects it to higher-rank propagators via interaction kernels. The most relevant are the two-time, or two-point, CFs: the particle-hole propagator, or response function, and the particle-particle, or fermionic pair, propagator. As we will see in the following, these CFs figure in the leading beyond-mean-field contributions to the fermionic self-energy, introducing the coupling of single-particle motion to collective degrees of freedom. The latter ones emerge as correlated (quasi)particle pairs forming boson-like structures exchanged between fermions. This phenomenon is known as (quasi)particle-vibration coupling, or (quasi)particle-phonon coupling, while the quasi-bosons, or phonons, associated with the response and pair CFs, underly the zero sound and superfluidity phenomena, respectively. Besides their in-medium realm, the phonons also exist on-shell in the form of collective normal and pairing vibrations, which can be actualized by electromagnetic, hadronic, and weak probes or by nucleon pair transfer in the case of pairing.

The particle-hole propagator, or response, is defined as:

$$R(12, 1'2') \equiv R_{12, 1'2'}(t - t') = -i \langle T \psi^\dagger(1) \psi(2) \psi^\dagger(2') \psi(1') \rangle \\ = -i \langle T (\psi_1^\dagger \psi_2)(t) (\psi_2^\dagger \psi_{1'}) (t') \rangle, \quad (9)$$

and the pair propagator reads:

$$G(12, 1'2') \equiv G_{12, 1'2'}(t - t') = -i \langle T \psi(1) \psi(2) \psi^\dagger(2') \psi^\dagger(1') \rangle \\ = -i \langle T (\psi_1 \psi_2)(t) (\psi_2^\dagger \psi_{1'}^\dagger)(t') \rangle. \quad (10)$$

Both CFs, like the single-particle propagator, depend on a single time difference, and it is implied that $t_1 = t_2 = t, t_{1'} = t_{2'} = t'$.

After inserting the completeness relation between the operator pairs and performing the Fourier transformations, analogously to the one-fermion case, the spectral expansions of CFs (9,10) turn out to be the following series:

$$R_{12, 1'2'}(\omega) = \sum_{\nu > 0} \left[\frac{\rho_{21}^\nu \rho_{2'1'}^{\nu*}}{\omega - \omega_\nu + i\delta} - \frac{\rho_{12}^{\nu*} \rho_{1'2'}}{\omega + \omega_\nu - i\delta} \right] \quad (11)$$

$$G_{12, 1'2'}(\omega) = \sum_\mu \frac{\alpha_{21}^\mu \alpha_{2'1'}^{\mu*}}{\omega - \omega_\mu^{(++)} + i\delta} - \sum_\varkappa \frac{\beta_{12}^{\varkappa*} \beta_{1'2'}}{\omega + \omega_\varkappa^{(--) - i\delta}, \quad (12)$$

similarly local and unitary, as higher operator rank two-point CFs. The poles are located at the energies $\omega_\nu = E_\nu - E_0, \omega_\mu^{(++)} = E_\mu^{(N+2)} - E_0^{(N)}$, and $\omega_\varkappa^{(--) = E_\varkappa^{(N-2)} - E_0^{(N)}$ of the systems with N and $N \pm 2$ particles, respectively. The sums in Eqs. (7,11,12) are formally complete, i.e., include both the discrete and continuum states.

The residues are products of the matrix elements

$$\rho_{12}^\nu = \langle 0 | \psi_2^\dagger \psi_1 | \nu \rangle \quad (13)$$

$$\alpha_{12}^\mu = \langle 0^{(N)} | \psi_2 \psi_1 | \mu^{(N+2)} \rangle \quad \beta_{12}^{\varkappa} = \langle 0^{(N)} | \psi_2^\dagger \psi_1^\dagger | \varkappa^{(N-2)} \rangle \quad (14)$$

which are the normal ρ_{12}^ν and anomalous (pairing) $\alpha_{12}^\mu, \beta_{12}^{\varkappa}$ transition densities, i.e., the weights of the pure particle-hole, two-particle and two-hole configurations on top of the ground state $|0^{(N)}\rangle$ in the excited states of the respective systems. The transition densities characterize transition probabilities, pair transfer amplitudes, and superfluid pairing spectral gaps [26]. We note here that Eqs. (7,11 - 14) are model-independent, i.e., remain valid for any reasonable approximations to the many-body states $|n\rangle, |m\rangle, |\nu\rangle, |\mu\rangle$, and $|\varkappa\rangle$.

B. Equation of motion for the single-fermion propagator: the normal phase

The canonical way of generating the EOM for the fermionic propagator (6) in the Hamiltonian formalism is taking time derivatives with respect to the time variables. Here, we navigate the reader through the major steps, while the detailed derivation can be found in Refs. [17, 46], in agreement with earlier work [7, 12-14, 95-97].

Differentiating Eq. (6) with respect to t gives:

$$\partial_t G_{11'}(t - t') = -i\delta(t - t') \langle [\psi_1(t), \psi_{1'}^\dagger(t')] \rangle_+ + \langle T [H, \psi_1](t) \psi_{1'}^\dagger(t') \rangle, \quad (15)$$

where we denote, to simplify the notations, the time-dependent operator products and, in particular, the commutator as $[H, \psi_1](t) = e^{iHt}[H, \psi_1]e^{-iHt}$. First, the commutator with the one-body part of the Hamiltonian is evaluated explicitly. Then, isolating $G_{11'}(t-t')$, one obtains the equation:

$$(i\partial_t - \varepsilon_1)G_{11'}(t-t') = \delta_{11'}\delta(t-t') + i\langle T[V, \psi_1](t)\psi^\dagger_{1'}(t') \rangle. \quad (16)$$

Second, the commutator with the interacting two-body part is evaluated, which leads to the first EOM, or EOM1:

$$(i\partial_t - \varepsilon_1)G_{11'}(t-t') = \delta_{11'}\delta(t-t') + \frac{i}{2} \sum_{ikl} \bar{v}_{ikl} \langle T(\psi_i^\dagger \psi_l \psi_k)(t)\psi^\dagger_{1'}(t') \rangle, \quad (17)$$

where the Latin dummy indices have the same meaning as the number indices and mark the intermediate fermionic states in the working single-particle basis. Eq. (17) is the most common form of the single-particle propagator EOM [7, 89, 97]. The two-fermion CF on the right-hand side of Eq. (17) is the heart of the dynamical interaction kernel which signals that the one-fermion propagator and the associated properties are coupled to higher-rank propagators. An EOM for this two-fermion CF can be generated, but its dynamical kernel contains a further higher-rank CF forming a complex hierarchy which is the characteristic feature of strongly-correlated systems described in the QFT language. In weakly coupled regimes, i.e., when the interaction V contains a small parameter, the perturbation theory is a viable solution that has the advantage of controllability and quantifiable uncertainties, however, perturbative expansions do not converge at strong coupling.

The latter is the case of nuclear systems, therefore, we focus on non-perturbative solutions in this discourse. The Fourier image of Eq. (17) reads

$$G_{11'}(\omega) = G_{11'}^0(\omega) + \frac{1}{2} \sum_{2ikl} G_{12}^0(\omega) \bar{v}_{2ikl} G_{ilk,1'}^{(2)}(\omega), \quad (18)$$

where we introduced $G_{11'}^0(\omega) = \delta_{11'}/(\omega - \varepsilon_1)$, which plays the role of the free, or uncorrelated, fermionic propagator, and the CF $G_{ilk,1'}^{(2)}$ on the right-hand side is the Fourier image of

$$G_{ilk,1'}^{(2)}(t-t') = -i\langle T(\psi_i^\dagger \psi_l \psi_k)(t)\psi^\dagger_{1'}(t') \rangle. \quad (19)$$

Eq. (18) can be further transformed to the Dyson form [96, 97]. There exist various approximations to the integral part of the Eq. (18), specifically to the CF $G^{(2)}$. The relativistic " Λ^{00} , Λ^{10} ", and " Λ^{11} " approximations are known from, e.g., Refs. [90]. They are based on factorizing the CF (19) into two one-fermion CFs (6) of correlated or uncorrelated character. Another common approach is known as the Gor'kov theory of superfluidity which retains, in addition, one-fermion CFs with the

same kind of field operators (anomalous Green functions) in the one-fermion CFs [8, 98]. The detailed derivation of the Gor'kov theory from Eq. (18) can be found in Ref. [46].

Before elaborating on feasible non-perturbative solutions of Eq. (17), we transform it into a symmetric form, which provides more insights into the interacting part of the one-fermion EOM. This form is obtained by differentiating the last term on the right-hand side of Eq. (16) $R_{11'}(t-t') = i\langle T[V, \psi_1](t)\psi^\dagger_{1'}(t') \rangle$ with respect to t' :

$$R_{11'}(t-t')\overleftarrow{\partial}_{t'} = -i\delta(t-t')\langle [[V, \psi_1](t), \psi^\dagger_{1'}(t')]_+ \rangle - \langle T[V, \psi_1](t)[H, \psi^\dagger_{1'}(t')] \rangle, \quad (20)$$

which leads to the EOM2:

$$(17) \quad R_{11'}(t-t')(-i\overleftarrow{\partial}_{t'} - \varepsilon_{1'}) = -\delta(t-t')\langle [[V, \psi_1](t), \psi^\dagger_{1'}(t')]_+ \rangle + i\langle T[V, \psi_1](t)[V, \psi^\dagger_{1'}(t')] \rangle. \quad (21)$$

Acting on the EOM1 (16) by the operator $(-i\overleftarrow{\partial}_{t'} - \varepsilon_{1'})$ and performing the Fourier transformation, one obtains:

$$G_{11'}(\omega) = G_{11'}^0(\omega) + \sum_{22'} G_{12}^0(\omega) T_{22'}(\omega) G_{2'1'}^0(\omega), \quad (22)$$

with $T(\omega)$ being the Fourier image of the time-dependent T -matrix:

$$\begin{aligned} T_{11'}(t-t') &= T_{11'}^0(t-t') + T_{11'}^r(t-t'), \\ T_{11'}^0(t-t') &= -\delta(t-t')\langle [[V, \psi_1](t), \psi^\dagger_{1'}(t')]_+ \rangle, \\ T_{11'}^r(t-t') &= i\langle T[V, \psi_1](t)[V, \psi^\dagger_{1'}(t')] \rangle. \end{aligned} \quad (23)$$

According to Eq. (22), the complete in-medium one-fermion propagator G is expressed via the free propagator G^0 and the T -matrix (23), which includes all possible interaction processes of a single fermion with the correlated medium. It is fundamentally split into the static, or instantaneous, part T^0 and dynamical, or time-dependent, part T^r containing retardation effects. The EOM (22) is more convenient in the Dyson form operating the irreducible part of the T -matrix with respect to the uncorrelated one-fermion propagator G^0 . The irreducible part of the T -matrix is the self-energy (called also interaction kernel): $\Sigma = T^{irr}$ defined via:

$$T(\omega) = \Sigma(\omega) + \Sigma(\omega)G^0(\omega)T(\omega). \quad (24)$$

Combining Eq. (22) in the operator form

$$G(\omega) = G^0(\omega) + G^0(\omega)T(\omega)G^0(\omega) \quad (25)$$

and (24), the Dyson equation for the fermionic propagator is obtained as:

$$G(\omega) = G^0(\omega) + G^0(\omega)\Sigma(\omega)G(\omega). \quad (26)$$

The self-energy inherits the decomposition into the static and dynamical contributions from the T -matrix:

$$\Sigma_{11'}(\omega) = \Sigma_{11'}^0 + \Sigma_{11'}^r(\omega), \quad (27)$$

which can be specified after evaluating the commutators of Eqs. (23), namely

$$\Sigma_{11'}^0 = -\langle [[V, \psi_1], \psi^\dagger_{1'}]_+ \rangle = \sum_{il} \bar{v}_{1i1'l} \rho_{li}, \quad \rho_{li} = \langle \psi^\dagger_i \psi_l \rangle \quad (28)$$

with ρ_{li} being the matrix elements of the ground-state one-body density, and $\Sigma_{11'}^r(\omega)$ as the Fourier transform of

$$\begin{aligned} \Sigma_{11'}^r(t-t') &= -\frac{i}{4} \sum_{npq} \sum_{ikl} \bar{v}_{1ikl} \times \\ &\times \langle T(\psi_i^\dagger \psi_l \psi_k)(t) (\psi_p^\dagger \psi_q^\dagger \psi_n)(t') \rangle^{irr} \bar{v}_{qpn1'} \\ &= \frac{1}{4} \sum_{npq} \sum_{ikl} \bar{v}_{1ikl} G_{ilk, nqp}^{(pph)irr}(t-t') \bar{v}_{qpn1'}. \end{aligned} \quad (29)$$

The static part Σ^0 (28), or the mean field, has the famous Hartree-Fock ansatz with, in general, correlated density, and the clearly separated dynamical part Σ^r has, in this formulation, the symmetric form of a three-fermion CF "sandwiched" between two interaction matrix elements. Respectively, the former generates short-range correlations and the latter is responsible for the long-range ones. In this context, the short range is associated with the range of the bare interaction \bar{v} , and the long range extends to the size of the entire many-body system. Eq. (26) is formally a closed exact equation for $G(\omega)$, however, it is complicated by the three-fermion CF in the dynamical kernel.

The analogous EOM method for the three-body two-time propagator generates a similar Dyson-type equation with static and dynamical self-energies. The latter is a function of even higher-rank propagators, which makes the exact solution of the many-body problem hardly tractable. Instead, approximations to the three-fermion propagator are considered. Within the non-perturbative paradigm, the cluster decomposition of the two-particle-one-hole CF in the dynamical kernel (29) is one of the viable approaches. Symbolically, it takes the form:

$$G^{(pph)irr} \sim G^{(p)} G^{(p)} G^{(h)} + G^{(p)} R^{(ph)} + G^{(h)} G^{(pp)} + \sigma^{(pph)}, \quad (30)$$

where the number of particles (p) and holes (h) in the superscripts indicates the rank of the respective CF, and the sum implicitly includes all the necessary antisymmetrizations. An accurate decomposition is given and discussed, e.g., in Refs. [17, 99, 100]. Retaining the first term only truncates the many-body problem at the one-body level, which constitutes the self-consistent Green functions approach. Some implementations were presented in Refs. [89, 90]. The one-fermion EOM then has a manifestly closed form and can be solved iteratively. The next level of sophistication is decomposition, retaining all possible terms with one-fermion and two-fermion propagators, i.e., the second and third terms in Eq. (30). This class of solutions can be mapped to the PVC [5, 17, 99–102], including the coupling between

particles and phonons of both particle-hole and particle-particle origins, and linked to the nuclear field theory [28–32].

The PVC concept will be the central one in the applications discussed in this course. Therefore, we dwell on its mathematical aspects and derive the explicit form of the PVC self-energy. After performing the decomposition (30) and dropping the last term (its role and quantitative contribution are commented on below), the one-fermion dynamical kernel takes the form

$$\Sigma_{11'}^r(\omega) = \Sigma_{11'}^{r(ph)}(\omega) + \Sigma_{11'}^{r(pp)}(\omega) + \Sigma_{11'}^{r(0)}(\omega). \quad (31)$$

The three terms on the right-hand side marked by '(ph)', '(pp)', and '(0)' are ordered according to their importance for typical nuclear structure calculations and correspond to the second, third, and first terms of Eq. (30), respectively. Explicitly, after performing the factorizations and Fourier transformations of the CF products to the energy domain, they read:

$$\begin{aligned} \Sigma_{11'}^{r(ph)}(\omega) &= \sum_{33'} \left[\sum_{\nu n} \frac{\eta_3^n g_{13}^\nu g_{1'3'}^{\nu*} \eta_{3'}^{n*}}{\omega - \omega_\nu - \varepsilon_n^{(+)} + i\delta} + \right. \\ &\left. + \sum_{\nu m} \frac{\chi_3^m g_{31}^{\nu*} g_{3'1'}^\nu \chi_{3'}^{m*}}{\omega + \omega_\nu + \varepsilon_m^{(-)} - i\delta} \right], \end{aligned} \quad (32)$$

$$\begin{aligned} \Sigma_{11'}^{r(pp)}(\omega) &= \sum_{22'} \left[\sum_{\mu m} \frac{\chi_2^{m*} \gamma_{12}^{\mu(+)} \gamma_{1'2'}^{\mu(+)*} \chi_{2'}^m}{\omega - \omega_\mu^{(++)} - \varepsilon_m^{(-)} + i\delta} + \right. \\ &\left. + \sum_{\varkappa n} \frac{\eta_2^{n*} \gamma_{21}^{\varkappa(-)*} \gamma_{2'1'}^{\varkappa(-)} \eta_{2'}^n}{\omega + \omega_\varkappa^{(--)} + \varepsilon_n^{(+)} - i\delta} \right], \end{aligned} \quad (33)$$

$$\begin{aligned} \Sigma_{11'}^{r(0)}(\omega) &= - \sum_{2342'3'4'} \bar{v}_{1234} \times \\ &\times \left[\sum_{mn'n''} \frac{\chi_2^m \chi_2^{m*} \eta_3^{n'} \eta_{3'}^{n'*} \eta_4^{n''} \eta_{4'}^{n''*}}{\omega - \varepsilon_{n'}^{(+)} - \varepsilon_{n''}^{(+)} - \varepsilon_m^{(-)} + i\delta} \right. \\ &\left. + \sum_{nm'm''} \frac{\eta_2^n \eta_2^{n*} \chi_3^{m'} \chi_{3'}^{m'*} \chi_4^{m''} \chi_{4'}^{m''*}}{\omega + \varepsilon_n^{(+)} + \varepsilon_{m'}^{(-)} + \varepsilon_{m''}^{(-)} - i\delta} \right] \bar{v}_{4'3'2'1'}, \end{aligned} \quad (34)$$

where $\varepsilon_n^{(+)} = E_n^{(N+1)} - E_0^{(N)}$ are the single-particle energies in the neighboring $(N+1)$ -particle system and $\varepsilon_m^{(-)} = E_m^{(N-1)} - E_0^{(N)}$ are those in the $(N-1)$ -particle system.

Mapping onto the PVC constitutes an important step that enables a reformulation of the many-body theory as an effective field theory. Unlike in most of the effective field theories, we can perform the mapping exactly by introducing the phonon degrees of freedom via the interaction amplitudes Γ^{ph} and Γ^{pp} :

$$\begin{aligned} \Gamma_{13',1'3}^{ph} &= \sum_{242'4'} \bar{v}_{1234} R_{24,2'4'}^{(ph)}(\omega) \bar{v}_{4'3'2'1'} = \\ &= \sum_{\nu, \sigma=\pm 1} g_{13}^{\nu(\sigma)} D_\nu^{(\sigma)}(\omega) g_{1'3'}^{\nu(\sigma)*}, \end{aligned} \quad (35)$$

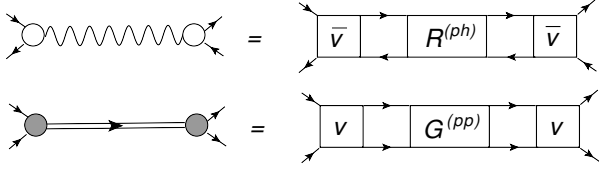


FIG. 1. The PVC "anatomy": the normal (top) and superfluid (bottom) phonon vertices are denoted by the empty and filled circles, respectively, the wavy and double lines stand for their propagators. The bare interaction, antisymmetrized \bar{v} and plain v , is represented by the squares, and the two-fermion correlation functions are given by the rectangular blocks $R^{(ph)}$ and $G^{(pp)}$. Solid lines are associated with fermionic particle (right arrows) and hole (left arrows) states with respect to the Fermi energy. The figure is adopted from Ref. [17].

$$\begin{aligned} \Gamma_{12,1'2'}^{pp}(\omega) &= \sum_{343'4'} v_{1234} G_{43,3'4'}^{(pp)}(\omega) v_{4'3'2'1'} = \\ &= \sum_{\mu, \sigma = \pm 1} \tilde{\gamma}_{12}^{\mu(\sigma)} \Delta_{\mu}^{(\sigma)}(\omega) \tilde{\gamma}_{1'2'}^{\mu(\sigma)*}. \end{aligned} \quad (36)$$

The vertices of the normal (zero-sound) phonons g^{ν} and their propagators $D_{\nu}(\omega)$ are, thereby:

$$g_{13}^{\nu(\sigma)} = \delta_{\sigma,+1} g_{13}^{\nu} + \delta_{\sigma,-1} g_{31}^{\nu*}, \quad g_{13}^{\nu} = \sum_{24} \bar{v}_{1234} \rho_{42}^{\nu}, \quad (37)$$

$$D_{\nu}^{(\sigma)}(\omega) = \frac{\sigma}{\omega - \sigma(\omega_{\nu} - i\delta)}, \quad \omega_{\nu} = E_{\nu} - E_0, \quad (38)$$

and those for the superfluid pairing phonons $\gamma^{\mu(\pm)}$ and $\Delta_{\mu}(\omega)$, respectively, read:

$$\begin{aligned} \tilde{\gamma}_{12}^{\mu(\sigma)} &= \gamma_{12}^{\mu(+)} \delta_{\sigma,+1} + \gamma_{12}^{\mu(-)*} \delta_{\sigma,-1}, \\ \gamma_{12}^{\mu(+)} &= \sum_{34} v_{1234} \alpha_{34}^{\mu}, \quad \gamma_{12}^{\mu(-)} = \sum_{34} \beta_{34}^{\mu} v_{3412}, \end{aligned} \quad (39)$$

$$\Delta_{\mu}^{(\sigma)}(\omega) = \frac{\sigma}{\omega - \sigma(\omega_{\mu}^{(\sigma\sigma)} - i\delta)}. \quad (40)$$

In the expressions above, the particle-particle (pp) and particle-hole (ph) correlation functions of Eqs. (9, 10) are employed. The PVC mappings introduced by Eqs. (35, 36) are displayed diagrammatically in Fig. 1.

The mappings (35, 36) can further link the spectral expansions (32 – 34) to the diagrammatic form of the dynamical self-energy shown in Fig. 2. Here we notice that its three terms correspond to two one-loop and one two-loop diagrams which may be linked to the Feynman diagrams and, thus, evaluated by the Feynman rules:

$$\Sigma_{11'}^{r(ph)}(\omega) = - \sum_{33'} \int_{-\infty}^{\infty} \frac{d\varepsilon}{2\pi i} \Gamma_{13',1'3}^{ph}(\omega - \varepsilon) G_{33'}(\varepsilon), \quad (41)$$

$$\Sigma_{11'}^{r(pp)}(\omega) = \sum_{22'} \int_{-\infty}^{\infty} \frac{d\varepsilon}{2\pi i} \Gamma_{12,1'2'}^{pp}(\omega + \varepsilon) G_{2'2}(\varepsilon), \quad (42)$$

$$\begin{aligned} \Sigma_{11'}^{r(0)}(\omega) &= - \sum_{2342'3'4'} \bar{v}_{1234} \\ &\times \int_{-\infty}^{\infty} \frac{d\varepsilon d\varepsilon'}{(2\pi i)^2} G_{44'}(\omega + \varepsilon' - \varepsilon) G_{33'}(\varepsilon) G_{2'2}(\varepsilon') \\ &\times \bar{v}_{4'3'2'1'}. \end{aligned} \quad (43)$$

Here, we make a remark that the signs in front of the diagrams may be convention-dependent. For instance, the last term is often shown with the "-" sign in the literature because this sign shows up explicitly in Eq. (34). Furthermore, the phonon vertices may include phase factors. The first two diagrams on the right-hand side in Fig. 2 are analogous to the electron self-energy lowest-order correction in quantum electrodynamics. For electronic systems, this term corresponds to the emission and reabsorption of a virtual photon or a phonon excitation of the lattice in a solid. In quantum hadrodynamics, a single nucleon emits and reabsorbs mesons of various kinds, which in the lowest order is the first diagram on the right-hand side, if the wavy line is attributed to the meson propagator. In the nuclear structure applications, the one-meson exchange acts as a bare interaction (or that with slightly renormalized coupling constants), while multiple in-medium meson-exchange processes are generated by the EOM non-perturbatively. In a strong coupling regime, the leading approximation is dominated by the term $\Sigma^{r(ph)}$ (32), which takes the form analogous to the boson exchange, thereby illustrating how the fermionic interaction is driven across the energy scales. The possibility of the PVC mapping signals the appearance of the new order parameter associated with the coupling vertex, which *takes over the power counting governing the bare nucleon-nucleon interaction evaluated with the vacuum averages*. In the many-body system, the latter is replaced by the ground-state averages, which provide an adequate framework where the description can be organized around the mean field emerging from collective effects.

After the PVC mapping, an effective Hamiltonian with explicit phonon degrees of freedom can be introduced, leading to NFT, the theory of nucleons and phonons in a correlated medium. In contrast to QFTs, where the coupled fermionic and bosonic degrees of freedom are independent, in NFT, the phonons are composed of correlated fermionic pairs. Furthermore, as we have seen, the PVC vertices in nuclear systems are not the effective parameters of the theory but are, in principle, calculable from the underlying fermionic bare interaction, i.e., NFT can be "ultraviolet (UV) complete" up to the underlying bare NN interaction defined for nucleons in the vacuum. Of course, in our case, all the expectation values are for-

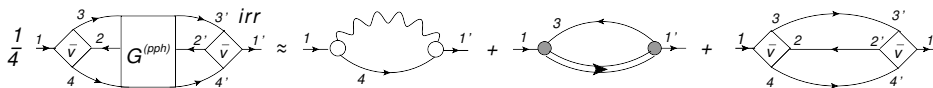


FIG. 2. The dynamical self-energy (kernel Σ^r of Eq. (31) in terms of PVC, using the same conventions as in Fig. 1. The block $G^{(pph)}$ represents the three-fermion propagator of Eq. (29). The figure is adopted from Ref. [17].

mally taken in correlated many-body states, while QFTs operate vacuum averages.

Some realizations of the PVC model based on the bare NN interaction are available in Refs. [103, 104]. Quantitatively, implementations that use effective interactions [53–55, 105] are more accurate in comparison to data. They are also easier to implement because the phonons can be reasonably described on the one-loop level of (quasiparticle) random phase approximation ((Q)RPA), therefore, arduous successive iterations of the fermionic propagator in the Dyson equation can be avoided. Such approaches inevitably imply an additional procedure to remove the double counting of PVC, implicitly contained in the effective interaction. A relatively simple yet elegant way of avoiding such double counting is the explicit subtraction of the dynamical PVC kernel taken in the static limit from the effective interaction [39]. The subtraction method is widely applied in calculations of two-nucleon Green functions, in particular, the particle-hole response [17, 36, 39–41, 69].

Resuming the discussion of the complete dynamical kernel (31), in theory, truncated on the two-body level, it requires information about the two-fermion propagators $R^{(ph)}$ and $G^{(pp)}$ and the phonon vertices and propagators. The latter can be obtained from their direct computation by solving the EOMs for these CFs. The theory and implementations of the corresponding EOMs are presented, e.g., in Refs. [14, 17, 23, 26]. The response theory is the subject of Section IID, and its implementations are discussed in Section III.

The consequence of the different sign in front of the "second-order" term $\Sigma^{r(0)}$, as compared to the "radiative correction" terms $\Sigma^{r(ph)}$ and $\Sigma^{r(pp)}$ containing phonons, is that potentially the positivity can be violated in the optical theorem. As it was pointed out, e.g., in Refs. [13, 106], keeping the integrity of the spectral representation of the dynamical self-energy (29)

$$\begin{aligned} \Sigma_{11'}^r(\omega) &= \frac{1}{4} \sum_{rpq} \sum_{ikl} \bar{v}_{1ikl} G_{ilk,rqp}^{(pph)irr}(\omega) \bar{v}_{qpr1'} \\ G_{ilk,rqp}^{(pph)}(\omega) &= \sum_n \frac{\langle 0 | \psi_i^\dagger \psi_l \psi_k | n \rangle \langle n | \psi_p^\dagger \psi_q^\dagger \psi_r | 0 \rangle}{\omega - (E_n^{(N+1)} - E_0^{(N)}) + i\delta} \\ &+ \sum_m \frac{\langle 0 | \psi_p^\dagger \psi_q^\dagger \psi_r | m \rangle \langle m | \psi_i^\dagger \psi_l \psi_k | 0 \rangle}{\omega + (E_m^{(N-1)} - E_0^{(N)}) - i\delta}. \end{aligned} \quad (44)$$

is important to prevent this violation. Finding viable approximations for the irreducible part of $G^{(pph)}$ com-

patible with the spectral expansion (44) was considered in the past. One of the possibilities was the two-particle-one-hole ($2p1h$) RPA for this correlation function [106], while another dwelled on a more accurate approximation to the $2p1h$ energies and matrix elements via Faddeev series [13]. The importance of including emergent collectivity in the ph and pp channels was particularly recognized. Numerical implementations for nuclear structure were also performed within the Tamm-Dancoff and random phase approximations to the ph and pp CFs [102–104, 107].

C. Single-fermion EOM in the superfluid phase

Superfluidity is a pronounced emergent property of strongly correlated fermionic systems, including atomic nuclei [101]. The inclusion of superfluidity requires an extended treatment on the theory side. The superfluid phase of fermionic systems exhibits an enhanced formation of Cooper pairs and their dynamical counterparts pairing phonons. The latter already appeared in the $\Sigma^{r(pp)}$ part of the fermionic dynamical self-energy derived in the previous subsection. When an effective interaction is used to describe the static part of the NN in-medium self-energy, the quantitative contribution of the pairing term is smaller than that of $\Sigma^{r(ph)}$ in the nuclear systems with double shell closure where the formation of the pairing gaps is suppressed by large shell gaps. It is, however, enhanced in open-shell systems, and the relative importance of $\Sigma^{r(pp)}$ and $\Sigma^{r(ph)}$ may change in computation with a bare interaction. Moreover, these two terms form a multi-component structure that can be unified in the formalism of Bogolyubov's quasiparticles. In the PVC approach discussed above, the superfluid pairing is fully dynamic as it is mediated by the pairing phonons emerging in the one-fermion self-energy from the bare interaction. In a framework based on effective interaction, the superfluid pairing can be included statically in the Bardeen-Cooper-Schrieffer (BCS) approximation or the Hartree-(Fock)-Bogolyubov one. The corresponding Green function technique is the Gor'kov Green function, which extends the notion of the one-fermion propagator (6) by introducing anomalous components with the same kind of fermionic operators, which is done below. These CFs are non-negligible because of the presence of correlated fermionic pairs in the ground state of the system. We will also see that more two-body CFs should be retained in the dynamical self-energy.

The simplest approach to the single-fermion motion with superfluidity can be obtained from the EOM1 neglecting two-body and higher-rank CFs [8]. In Ref. [46], Gor'kov theory is generalized beyond this approximation to the inclusion of the PVC effects. Here we briefly discuss this approximation, for which it is convenient to introduce the HFB basis, or the basis of the Bogolyubov quasiparticles [108]. The single-fermion states in this basis are superpositions of particles and holes, i.e., the fermionic states above and below the Fermi energy:

$$\begin{aligned}\psi_1 &= \sum_{\mu} (U_{1\mu}\alpha_{\mu} + V_{1\mu}^*\alpha_{\mu}^{\dagger}) \\ \psi_1^{\dagger} &= \sum_{\mu} (V_{1\mu}\alpha_{\mu} + U_{1\mu}^*\alpha_{\mu}^{\dagger}),\end{aligned}\quad (45)$$

where α and α^{\dagger} are the quasiparticle operators obeying the same anticommutator algebra as the particle operators ψ and ψ^{\dagger} . Here and henceforth, the Greek indices denote fermionic states in the HFB basis, and the number and Roman indices are reserved for the single-particle mean-field basis states. Eq. (45) can be written in a matrix form:

$$\begin{pmatrix} \psi \\ \psi^{\dagger} \end{pmatrix} = \mathcal{W} \begin{pmatrix} \alpha \\ \alpha^{\dagger} \end{pmatrix}, \quad (46)$$

where

$$\mathcal{W} = \begin{pmatrix} U & V^* \\ V & U^* \end{pmatrix} \quad \mathcal{W}^{\dagger} = \begin{pmatrix} U^{\dagger} & V^{\dagger} \\ V^T & U^T \end{pmatrix} \quad (47)$$

are unitary matrices. The matrix blocks U and V satisfy [101]:

$$\begin{aligned}U^{\dagger}U + V^{\dagger}V &= \mathbb{1} & UU^{\dagger} + V^*V^T &= \mathbb{1} \\ U^TV + V^TU &= 0 & UV^{\dagger} + V^*U^T &= 0.\end{aligned}\quad (48)$$

It is convenient to consider a generalized four-component, or *quasiparticle*, fermionic propagator

$$\begin{aligned}\hat{G}_{12}(t-t') &= -i\langle T\Psi_1(t)\Psi_2^{\dagger}(t') \rangle = \\ &= -i\theta(t-t') \begin{pmatrix} \langle \psi_1(t)\psi_2^{\dagger}(t') \rangle & \langle \psi_1(t)\psi_2(t') \rangle \\ \langle \psi_1^{\dagger}(t)\psi_2^{\dagger}(t') \rangle & \langle \psi_1^{\dagger}(t)\psi_2(t') \rangle \end{pmatrix} + \\ &+ i\theta(t'-t) \begin{pmatrix} \langle \psi_2^{\dagger}(t')\psi_1(t) \rangle & \langle \psi_2(t')\psi_1(t) \rangle \\ \langle \psi_2^{\dagger}(t')\psi_1^{\dagger}(t) \rangle & \langle \psi_2(t')\psi_1^{\dagger}(t) \rangle \end{pmatrix} \\ &= \begin{pmatrix} G_{12}(t-t') & F_{12}^{(1)}(t-t') \\ F_{12}^{(2)}(t-t') & G_{12}^{(h)}(t-t') \end{pmatrix},\end{aligned}\quad (49)$$

via introducing

$$\Psi_1(t) = \begin{pmatrix} \psi_1(t) \\ \psi_1^{\dagger}(t) \end{pmatrix}, \quad \Psi_1^{\dagger}(t) = \begin{pmatrix} \psi_1^{\dagger}(t) & \psi_1(t) \end{pmatrix}.\quad (50)$$

The one-fermion EOM can be generated for all the components of the propagator (49) in a similar fashion as in the previous subsection. A compact unified EOM can

be obtained by transforming the resulting matrix equation for the \hat{G}_{12} to the quasiparticle basis [46], so the Gor'kov-Dyson equation for the quasiparticle propagator in the energy domain reads:

$$G_{\nu\nu'}^{(\eta)}(\varepsilon) = \tilde{G}_{\nu\nu'}^{(\eta)}(\varepsilon) + \sum_{\mu\mu'} \tilde{G}_{\nu\mu}^{(\eta)}(\varepsilon)\Sigma_{\mu\mu'}^{r(\eta)}(\varepsilon)G_{\mu'\nu'}^{(\eta)}(\varepsilon).\quad (51)$$

The indices $\eta = +$ and $\eta = -$ identify the quasiparticle forward and backward components, respectively.

The mean-field propagator $\tilde{G}_{\nu\nu'}^{(\eta)}(\varepsilon)$ absorbs the static kernel and can be made diagonal by a choice of the working basis:

$$\tilde{G}_{\nu\nu'}^{(\eta)}(\varepsilon) = \frac{\delta_{\nu\nu'}}{\varepsilon - \eta(E_{\nu} - E_0 - i\delta)},\quad (52)$$

while generally non-diagonal correlated propagator $G_{\nu\nu'}^{(\eta)}(\varepsilon)$ reads:

$$G_{\nu\nu'}^{(\eta)}(\varepsilon) = \sum_n \frac{S_{\nu\nu'}^{\eta(n)}}{\varepsilon - \eta(E_n - E_0 - i\delta)}.\quad (53)$$

In Eqs. (52, 53), E_{ν} are the mean-field energies of the Bogolyubov quasiparticles and E_n are the formally exact quasiparticle energies, affected by beyond-mean-field correlations. The residues $S_{\nu\nu'}^{\eta(n)}$ are the basis-dependent spectroscopic factors: $S_{\nu\nu'}^{+(n)} = \langle 0|\alpha_{\nu}|n\rangle\langle n|\alpha_{\nu'}^{\dagger}|0\rangle$ and $S_{\nu\nu'}^{-(n)} = \langle 0|\alpha_{\nu}|m\rangle\langle m|\alpha_{\nu'}^{\dagger}|0\rangle$ with the formally exact many-body states $|n\rangle$ and $|m\rangle$. The dynamical kernel in the quasiparticle basis is related to its single-particle basis representation as follows:

$$\begin{aligned}\Sigma_{\mu\mu'}^{r(+)}(\varepsilon) &= \sum_{12} \begin{pmatrix} U_{\mu 1}^{\dagger} & V_{\mu 1}^{\dagger} \end{pmatrix} \begin{pmatrix} \Sigma_{12}^r(\varepsilon) & \Sigma_{12}^{(1)r}(\varepsilon) \\ \Sigma_{12}^{(2)r}(\varepsilon) & \Sigma_{12}^{(h)r}(\varepsilon) \end{pmatrix} \begin{pmatrix} U_{2\mu'} \\ V_{2\mu'} \end{pmatrix} \\ &= \sum_{12} \left(U_{\mu 1}^{\dagger}\Sigma_{12}^r(\varepsilon)U_{2\mu'} + U_{\mu 1}^{\dagger}\Sigma_{12}^{(1)r}(\varepsilon)V_{2\mu'} \right. \\ &\quad \left. + V_{\mu 1}^{\dagger}\Sigma_{12}^{(2)r}(\varepsilon)U_{2\mu'} + V_{\mu 1}^{\dagger}\Sigma_{12}^{(h)r}(\varepsilon)V_{2\mu'} \right),\end{aligned}\quad (54)$$

$$\begin{aligned}\Sigma_{\mu\mu'}^{r(-)}(\varepsilon) &= \sum_{12} \begin{pmatrix} V_{\mu 1}^T & U_{\mu 1}^T \end{pmatrix} \begin{pmatrix} \Sigma_{12}^r(\varepsilon) & \Sigma_{12}^{(1)r}(\varepsilon) \\ \Sigma_{12}^{(2)r}(\varepsilon) & \Sigma_{12}^{(h)r}(\varepsilon) \end{pmatrix} \begin{pmatrix} V_{2\mu'}^* \\ U_{2\mu'}^* \end{pmatrix} \\ &= \sum_{12} \left(V_{\mu 1}^T\Sigma_{12}^r(\varepsilon)V_{2\mu'}^* + V_{\mu 1}^T\Sigma_{12}^{(1)r}(\varepsilon)U_{2\mu'}^* \right. \\ &\quad \left. + U_{\mu 1}^T\Sigma_{12}^{(2)r}(\varepsilon)V_{2\mu'}^* + U_{\mu 1}^T\Sigma_{12}^{(h)r}(\varepsilon)U_{2\mu'}^* \right),\end{aligned}\quad (55)$$

while the matrix structure of the dynamical self-energy corresponds to the structure of the propagator matrix (49).

The four time-dependent components of the exact dynamical self-energy in the single-particle basis are the double contractions of the three-fermion CFs with two interaction matrix elements:

$$\Sigma_{11'}^r(t-t') = \frac{i}{4} \sum_{ikl} \sum_{mnq} \bar{v}_{1ikl}$$

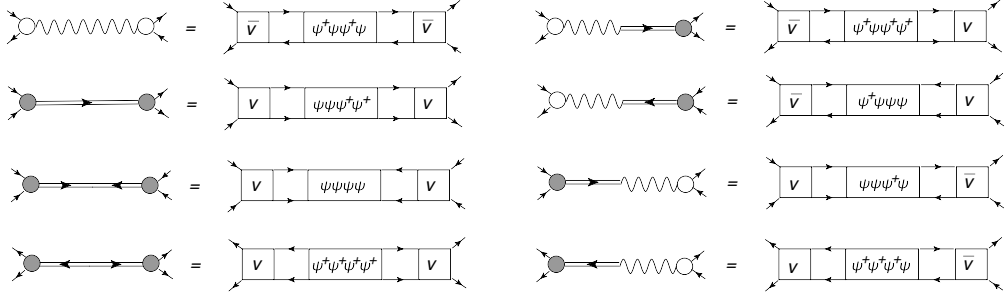


FIG. 3. The complete set of the quasiparticle-vibration coupling amplitudes in the diagrammatic form with the same conventions as in Figs. 1, 2. The depicted two-body two-point correlation functions are associated with the operator products given in the rectangular boxes, according to the rule: $\boxed{\text{abcd}} = -i\langle T(ab)(t)(cd)(t') \rangle$, and include the attached fermionic lines (arrowed lines). The figure is adopted from Ref. [109].

$$\begin{aligned}
& \times \langle T(\psi_i^\dagger \psi_l \psi_k)(t)(\psi_m^\dagger \psi_n^\dagger \psi_q)(t') \rangle^{irr} \bar{v}_{mnq1'} \\
\Sigma_{11'}^{(1)r}(t-t') &= \frac{i}{4} \sum_{ikl} \sum_{mnq} \bar{v}_{1ikl} \\
& \times \langle T(\psi_i^\dagger \psi_l \psi_k)(t)(\psi_m^\dagger \psi_q \psi_n)(t') \rangle^{irr} \bar{v}_{1'mnq}. \\
\Sigma_{11'}^{(2)r}(t-t') &= \frac{i}{4} \sum_{ikl} \sum_{mnq} \bar{v}_{ikl1} \\
& \times \langle T(\psi_i^\dagger \psi_k^\dagger \psi_l)(t)(\psi_m^\dagger \psi_n^\dagger \psi_q)(t') \rangle^{irr} \bar{v}_{mnq1'} \\
\Sigma_{11'}^{(h)r}(t-t') &= \frac{i}{4} \sum_{ikl} \sum_{mnq} \bar{v}_{ikl1} \\
& \times \langle T(\psi_i^\dagger \psi_k^\dagger \psi_l)(t)(\psi_m^\dagger \psi_q \psi_n)(t') \rangle^{irr} \bar{v}_{1'mnq}.
\end{aligned} \tag{56}$$

Similar to the normal case, each component of the superfluid dynamical kernel can be treated in various approximations. Following our program, we apply the general cluster decomposition (30) to the CFs of Eq. (56). At this point, one realizes that, in the superfluid ground state, more two-fermion CFs will give non-vanishing contributions. Namely, in the extension of the PVC approach to the superfluid, or quasiparticle, PVC dubbed as qPVC here and henceforth, the two-fermion propagators include the contributions collected in Fig. 3 in the diagrammatic representation. Accordingly, more of the corresponding EOMs should be supplied to the dynamical kernel, which may look overwhelming. However, rescue comes with transforming the Dyson equation to the quasiparticle basis (51 - 55). As a result of this transformation, the dynamical kernel $\Sigma_{\nu\nu'}^{r(+)}(\varepsilon)$ takes the form

$$\Sigma_{\nu\nu'}^{r(+)}(\varepsilon) = \sum_{\nu''\mu} \left[\frac{\Gamma_{\nu\nu''}^{(11)\mu} \Gamma_{\nu''\nu'}^{(11)\mu*}}{\varepsilon - E_{\nu''} - \omega_\mu + i\delta} + \frac{\Gamma_{\nu\nu''}^{(02)\mu*} \Gamma_{\nu''\nu'}^{(02)\mu}}{\varepsilon + E_{\nu''} + \omega_\mu - i\delta} \right], \tag{57}$$

where the entire multi-component structure of the two-

fermion GFs listed on the right-hand side of Fig. 3 becomes packed into the vertex functions $\Gamma^{(11)}$ and $\Gamma^{(02)}$ defined as follows:

$$\Gamma_{\nu\nu'}^{(11)\mu} = \sum_{12} \left[U_{\nu 1}^\dagger (g_{12}^\mu \eta_2^{\nu'} + \gamma_{12}^{\mu(+)} \chi_2^{\nu'*}) - V_{\nu 1}^\dagger ((g_{12}^\mu)^T \chi_2^{\nu'*} + (\gamma_{12}^{\mu(-)})^T \eta_2^{\nu'}) \right] \tag{58}$$

$$\Gamma_{\nu\nu'}^{(02)\mu} = - \sum_{12} \left[V_{\nu 1}^T (g_{12}^\mu \eta_2^{\nu'} + \gamma_{12}^{\mu(+)} \chi_2^{\nu'*}) - U_{\nu 1}^T ((g_{12}^\mu)^T \chi_2^{\nu'*} + (\gamma_{12}^{\mu(-)})^T \eta_2^{\nu'}) \right]. \tag{59}$$

The $\eta = -$ counterpart of Eq. (57) has an analogous form, however, in practice, it is redundant and has the same solution. The leading approximation implies the HFB values for the matrix elements η_i^ν and χ_i^ν , and Eqs. (58, 59) reduce to

$$\Gamma_{\nu\nu'}^{(11)\mu} = \left[U^\dagger g^\mu U + U^\dagger \gamma^{\mu(+)} V - V^\dagger g^{\mu T} V - V^\dagger \gamma^{\mu(-)T} U \right]_{\nu\nu'} \tag{60}$$

$$\Gamma_{\nu\nu'}^{(02)\mu} = - \left[V^T g^\mu U + V^T \gamma^{\mu(+)} V - U^T g^{\mu T} V - U^T \gamma^{\mu(-)T} U \right]_{\nu\nu'}. \tag{61}$$

Summarizing, we arrive at the compact form of the Gor'kov-Dyson equation (51) in the qPVC approximation, written in the basis of Bogolyubov quasiparticles. In this case, the dynamical kernel (57) has essentially the same form as in the non-superfluid case, and the complexity is transferred to the structure of the qPVC vertices (58, 59). The corresponding operation is shown in Fig. 4. Remarkably, in this framework, the normal and pairing phonons are unified in the superfluid phonons, whose vertices are linked to the variations of the quasiparticle

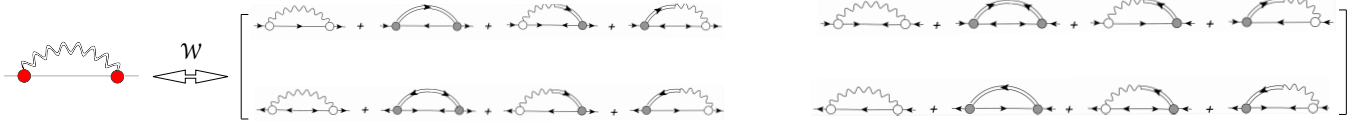


FIG. 4. The superfluid qPVC self-energy in the quasiparticle (left) and single-particle (right) bases related by Bogolyubov's transformation \mathcal{W} . The double wavy line stands for the propagator of a unified superfluid phonon in the quasiparticle basis, the filled (red) circles are reserved for the respective combined qPVC phonon vertices, and the single line without arrows is attributed to the quasiparticle propagator unifying particles and holes. The remaining conventions are kept intact with the preceding figures. The figure is adopted from Ref. [61].

Hamiltonian [46]. Solutions of Eq. (51) enable extraction of the single-particle characteristics of the many-body system. Refs. [54, 55] discuss the numerical solutions for spherical heavy nuclei, which allow for the shell evolution analyses and understanding of some features of spin-orbit splitting based on the "non-linear sigma" effective meson-exchange interactions adjusted within the covariant DFT (NL3 and NL3*) [110, 111]. Ref. [109] reports on an analogous implementation for axially deformed nuclei using the density-dependent meson exchange [112]. In both cases, the density of single-quasiparticle states is too small in the relativistic H(F)B mean-field approximation, and the inclusion of the dynamical kernels in the leading-order qPVC improves the description considerably.

D. The superfluid response theory

In the qPVC approach, the presence of the two-fermion propagators (9, 10) in the dynamical kernel Σ^r of the single-particle EOM (26, 51) requires the input in terms of these CFs, which is external to the single-particle EOM. In the explicit expressions for Σ^r (32, 33, 57), one finds qPVC vertices and phonon frequencies. The latter are the poles of the ph and pp ($2q$) propagators, and the former are obtained by contractions of the CFs residues with the bare fermionic interaction. The most direct way to obtain these elements of the qPVC amplitudes is to solve the EOMs for the CFs (9, 10). These EOMs were formulated, for instance, in Refs. [12, 14], and the PVC approximation to their dynamical kernels was discussed in Refs. [17, 25, 26]. The superfluid generalization of Eqs. (9, 10) must unify these propagators, however, in terms of Gor'kov Green functions (49), this becomes quite cumbersome because of the quickly increasing number of components. The previous subsection suggests that the formalism can become simpler in the quasiparticle basis. Therefore, we derive the EOMs for the two-fermion CFs in the quasiparticle space introduced by Eq. (45) from the beginning. The detailed derivation can be found in Ref. [61], and here I walk the reader through the major steps and outline feasible approximations of the qPVC class.

The Hamiltonian (1) takes the following form in the

quasiparticle basis [101]:

$$\begin{aligned}
 H = H^0 &+ \sum_{\mu\nu} H_{\mu\nu}^{11} \alpha_{\mu}^{\dagger} \alpha_{\nu} + \frac{1}{2} \sum_{\mu\nu} (H_{\mu\nu}^{20} \alpha_{\mu}^{\dagger} \alpha_{\nu}^{\dagger} + \text{h.c.}) \\
 &+ \sum_{\mu\mu'\nu\nu'} (H_{\mu\mu'\nu\nu'}^{40} \alpha_{\mu}^{\dagger} \alpha_{\mu'}^{\dagger} \alpha_{\nu}^{\dagger} \alpha_{\nu'}^{\dagger} + \text{h.c.}) \\
 &+ \sum_{\mu\mu'\nu\nu'} (H_{\mu\mu'\nu\nu'}^{31} \alpha_{\mu}^{\dagger} \alpha_{\mu'}^{\dagger} \alpha_{\nu}^{\dagger} \alpha_{\nu'} + \text{h.c.}) \\
 &+ \frac{1}{4} \sum_{\mu\mu'\nu\nu'} H_{\mu\mu'\nu\nu'}^{22} \alpha_{\mu}^{\dagger} \alpha_{\mu'}^{\dagger} \alpha_{\nu} \alpha_{\nu'}, \quad (62)
 \end{aligned}$$

where the upper indices in the Hamiltonian matrix elements $H_{\mu\nu}^{ij}$ and $H_{\mu\nu\mu'\nu'}^{ij}$ correspond to the numbers of creation and annihilation quasiparticle operators in the associated terms. The matrix elements H^{ij} in terms of the bare interaction and \mathcal{W} transformation coefficients can be found in [101]. The quantity H^{20} vanishes at the stationary point of the HFB equations, and the matrix elements of H^{11} are attributed to the quasiparticle energies, that is $H_{\mu\nu}^{11} = \delta_{\mu\nu} E_{\mu}$:

$$H = H^0 + \sum_{\mu} E_{\mu} \alpha_{\mu}^{\dagger} \alpha_{\mu} + V, \quad (63)$$

where the residual interaction V includes the remaining terms (the last three lines of Eq. (62)).

Now we depart from considering the closed system and subject it to an external field F , which is supposed to be sufficiently weak. Under this condition, the transitions of the many-body system to excited states can be treated in the lowest order perturbation theory (with respect to the field F). The strength function defined as

$$S(\omega) = \sum_{n>0} \left[|\langle n|F^{\dagger}|0\rangle|^2 \delta(\omega - \omega_n) - |\langle n|F|0\rangle|^2 \delta(\omega + \omega_n) \right], \quad (64)$$

where the summation runs over all the formally exact excited states $|n\rangle$, describes the spectral probability distribution.

The one-body operator F is canonically expanded in terms of the quasiparticle field operators:

$$F = \frac{1}{2} \sum_{\mu\mu'} \left(F_{\mu\mu'}^{20} \alpha_{\mu}^{\dagger} \alpha_{\mu'}^{\dagger} + F_{\mu\mu'}^{02} \alpha_{\mu} \alpha_{\mu'} \right)$$

$$F^\dagger = \frac{1}{2} \sum_{\mu\mu'} \left(F_{\mu\mu'}^{20*} \alpha_{\mu'} \alpha_\mu + F_{\mu\mu'}^{02*} \alpha_\mu^\dagger \alpha_{\mu'}^\dagger \right), \quad (65)$$

which is obtained via the Bogolyubov's transformation of the second-quantized form of $F = \sum_{12} F_{12} \psi_1^\dagger \psi_2$ after dropping the F^{00} term not generating excited states and F^{11} not contributing in the linear approximation [113]. Subleading contributions will be discussed elsewhere. Eq. (64) takes the form:

$$S(\omega) = -\frac{1}{\pi} \lim_{\Delta \rightarrow 0} \text{Im} \Pi(\omega),$$

$$\Pi(\omega) = \frac{1}{4} \sum_{\mu\mu'\nu\nu'} \left(F_{\mu\mu'}^{02} \quad F_{\mu\mu'}^{20} \right) \hat{\mathcal{R}}_{\mu\mu'\nu\nu'}(\omega + i\Delta) \begin{pmatrix} F_{\nu\nu'}^{02*} \\ F_{\nu\nu'}^{20*} \end{pmatrix}, \quad (66)$$

which sets the ansatz for the response function block matrix:

$$\begin{aligned} \hat{\mathcal{R}}_{\mu\mu'\nu\nu'}(\omega) &= \\ &= \sum_{n>0} \begin{pmatrix} \mathcal{X}_{\mu\mu'}^n \\ \mathcal{Y}_{\mu\mu'}^n \end{pmatrix} \frac{1}{\omega - \omega_n + i\delta} \begin{pmatrix} \mathcal{X}_{\nu\nu'}^{n*} & \mathcal{Y}_{\nu\nu'}^{n*} \end{pmatrix} \\ &- \sum_{n>0} \begin{pmatrix} \mathcal{Y}_{\mu\mu'}^{n*} \\ \mathcal{X}_{\mu\mu'}^{n*} \end{pmatrix} \frac{1}{\omega + \omega_n - i\delta} \begin{pmatrix} \mathcal{Y}_{\nu\nu'}^n & \mathcal{X}_{\nu\nu'}^n \end{pmatrix}, \end{aligned} \quad (67)$$

with the transition density components:

$$\mathcal{X}_{\mu\mu'}^n = \langle 0 | \alpha_{\mu'} \alpha_\mu | n \rangle \quad \mathcal{Y}_{\mu\mu'}^n = \langle 0 | \alpha_\mu^\dagger \alpha_{\mu'}^\dagger | n \rangle. \quad (68)$$

From Eq. (67), one deduces the time-dependent form of the superfluid response function as

$$\begin{aligned} \hat{\mathcal{R}}_{\mu\mu'\nu\nu'}(t-t') &= \\ &= -i \langle T \left(\begin{pmatrix} (\alpha_{\mu'} \alpha_\mu)(t) (\alpha_{\nu'}^\dagger \alpha_{\nu'}^\dagger)(t') & (\alpha_{\mu'} \alpha_\mu)(t) (\alpha_{\nu'} \alpha_{\nu'})(t') \\ (\alpha_\mu^\dagger \alpha_{\mu'}^\dagger)(t) (\alpha_\nu^\dagger \alpha_{\nu'}^\dagger)(t') & (\alpha_\mu^\dagger \alpha_{\mu'}^\dagger)(t) (\alpha_{\nu'} \alpha_{\nu'})(t') \end{pmatrix} \right) \rangle \\ &= -i \langle T \left(\begin{pmatrix} A_{\mu\mu'}(t) A_{\nu\nu'}^\dagger(t') & A_{\mu\mu'}(t) A_{\nu\nu'}(t') \\ A_{\mu\mu'}^\dagger(t) A_{\nu\nu'}^\dagger(t') & A_{\mu\mu'}^\dagger(t) A_{\nu\nu'}(t') \end{pmatrix} \right) \rangle, \end{aligned}$$

implying the time-dependent operator products in the Heisenberg picture:

$$\begin{aligned} A_{\mu\mu'}(t) &= (\alpha_{\mu'} \alpha_\mu)(t) = e^{iHt} \alpha_{\mu'} \alpha_\mu e^{-iHt} \\ A_{\nu\nu'}^\dagger(t) &= (\alpha_\nu^\dagger \alpha_{\nu'}^\dagger)(t) = e^{iHt} \alpha_\nu^\dagger \alpha_{\nu'}^\dagger e^{-iHt}. \end{aligned} \quad (70)$$

A Fourier transformation of Eq. (69) should yield Eq. (67) and vice versa to verify this. Here we also note that the response function is an internal characteristic of the many-body system disentangled from the strength function by Eq. (66).

The EOM for the superfluid response (69) is generated similarly to the EOMs for single-fermion propagators. Eq. (69) is differentiated sequentially with respect

to t and t' and, taking the Fourier image, one obtains

$$\begin{aligned} \hat{\mathcal{R}}_{\mu\mu'\nu\nu'}(\omega) &= \hat{\mathcal{R}}_{\mu\mu'\nu\nu'}^0(\omega) \\ &+ \frac{1}{4} \sum_{\gamma\gamma'\delta\delta'} \hat{\mathcal{R}}_{\mu\mu'\gamma\gamma'}^0(\omega) \hat{\mathcal{K}}_{\gamma\gamma'\delta\delta'}(\omega) \hat{\mathcal{R}}_{\delta\delta'\nu\nu'}(\omega), \end{aligned} \quad (71)$$

which is the Bethe-Salpeter equation but simplified to the Dyson form since the two-point CF is considered from the beginning. We will refer to it as Bethe-Salpeter-Dyson equation (BSDE). Eq. (71) has, however, in addition, the 2×2 matrix structure in the quasiparticle basis. The free (uncorrelated) response is defined as

$$\hat{\mathcal{R}}_{\mu\mu'\nu\nu'}^0(\omega) = [\omega - \hat{\sigma}_3 E_{\mu\mu'}]^{-1} \hat{\mathcal{N}}_{\mu\mu'\nu\nu'}, \quad (72)$$

$$E_{\mu\mu'} = E_\mu + E_{\mu'}, \quad \hat{\sigma}_3 = \begin{pmatrix} 1 & 0 \\ 0 & -1 \end{pmatrix}, \quad (73)$$

and the norm matrix $\hat{\mathcal{N}}_{\mu\mu'\nu\nu'}$, which is specified below. The static and dynamical parts of the interaction kernel $\hat{\mathcal{K}}(\omega) = \hat{\mathcal{K}}^0 + \hat{\mathcal{K}}^r(\omega)$ read:

$$\begin{aligned} \hat{\mathcal{K}}_{\gamma\gamma'\delta\delta'}^0 &= \frac{1}{4} \sum_{\eta\eta'\rho\rho'} \hat{\mathcal{N}}_{\gamma\gamma'\eta\eta'}^{-1} \hat{\mathcal{T}}_{\eta\eta'\rho\rho'}^0 \hat{\mathcal{N}}_{\rho\rho'\delta\delta'}^{-1} \\ \hat{\mathcal{K}}_{\gamma\gamma'\delta\delta'}^r(\omega) &= \frac{1}{4} \sum_{\eta\eta'\rho\rho'} \left[\hat{\mathcal{N}}_{\gamma\gamma'\eta\eta'}^{-1} \hat{\mathcal{T}}_{\eta\eta'\rho\rho'}^r(\omega) \hat{\mathcal{N}}_{\rho\rho'\delta\delta'}^{-1} \right]^{irr}, \end{aligned} \quad (74)$$

where the static and time-dependent $\hat{\mathcal{T}}$ -matrices in the quasiparticle space in the most general form are:

$$\begin{aligned} \hat{\mathcal{T}}_{\mu\mu'\nu\nu'}^0 &= - \left\langle \begin{pmatrix} [V, A_{\mu\mu'}], A_{\nu\nu'}^\dagger & [V, A_{\mu\mu'}], A_{\nu\nu'} \\ [V, A_{\mu\mu'}^\dagger], A_{\nu\nu'}^\dagger & [V, A_{\mu\mu'}^\dagger], A_{\nu\nu'} \end{pmatrix} \right\rangle \\ \hat{\mathcal{T}}_{\mu\mu'\nu\nu'}^r(t-t') &= i \times \\ &\times \langle T \left(\begin{pmatrix} [V, A_{\mu\mu'}](t) [V, A_{\nu\nu'}^\dagger](t') & [V, A_{\mu\mu'}](t) [V, A_{\nu\nu'}](t') \\ [V, A_{\mu\mu'}^\dagger](t) [V, A_{\nu\nu'}^\dagger](t') & [V, A_{\mu\mu'}^\dagger](t) [V, A_{\nu\nu'}](t') \end{pmatrix} \right) \rangle. \end{aligned} \quad (75)$$

The norm matrix $\hat{\mathcal{N}}_{\mu\mu'\nu\nu'}$ becomes, accordingly:

$$\hat{\mathcal{N}}_{\mu\mu'\nu\nu'} = \left\langle \begin{pmatrix} [A_{\mu\mu'}, A_{\nu\nu'}^\dagger] & 0 \\ 0 & [A_{\mu\mu'}^\dagger, A_{\nu\nu'}] \end{pmatrix} \right\rangle, \quad (77)$$

while its inverse is given by

$$\frac{1}{2} \sum_{\delta\delta'} \hat{\mathcal{N}}_{\mu\mu'\delta\delta'}^{-1} \hat{\mathcal{N}}_{\delta\delta'\nu\nu'} = \delta_{\mu\mu'\nu\nu'} = \delta_{\mu\nu} \delta_{\mu'\nu'} - \delta_{\mu\nu'} \delta_{\mu'\nu}. \quad (78)$$

The superfluid response theory is thus comprised of the BSDE (71) with the uncorrelated quasiparticle propagator (72) and interaction kernel (74) in their most general forms. At this point, the theory is still exact, but too general. To proceed further, the evaluation of the commutators figuring in Eqs. (75, 76, 76) is required. The exact forms of the ph and pp static kernels separately were presented and discussed, e.g., in Refs. [17, 24, 114]. Both contain the pure contribution of the bare fermionic interaction and its contractions with the correlated parts of the two-body fermionic densities. It is further pointed out that the latter densities are static limits of the two-fermion propagators, so that the correlated self-consistent static kernel contains feedback from the dynamical kernel. The superfluid analogs of these terms were not yet presented in the literature, and I will discuss them elsewhere. The ab-initio superfluid static kernel is the unification of the ph and pp static kernels which form the main diagonal of the block matrix (75). Dropping the correlated terms is technically confining by the HFB approximation. In this case, the superfluid static kernel simplifies to the kernel of QRPA. Its matrix elements are determined by the following expectation values [101]:

$$\begin{aligned} \langle \text{HFB} | [V, A_{\mu\mu'}], A_{\nu\nu'}^\dagger | \text{HFB} \rangle &= -H_{\mu\mu'\nu\nu'}^{22}, \\ \langle \text{HFB} | [[V, A_{\mu\mu'}], A_{\nu\nu'}] | \text{HFB} \rangle &= 4! H_{\mu\mu'\nu\nu'}^{40}, \\ \hat{\mathcal{N}}_{\mu\mu'\nu\nu'} &= \hat{\sigma}_3 \delta_{\mu\mu'\nu\nu'}, \end{aligned} \quad (79)$$

and the remaining matrix elements of Eq. (75) can be determined via Hermitian conjugation.

The dynamical kernel of Eq. (76) can be evaluated similarly and, in general, is quite complicated. The dominant contribution to the excited states comes from the diagonal components related as follows:

$$\mathcal{K}_{\mu\mu'\nu\nu'}^{r[22]}(\tau) = \mathcal{K}_{\nu\nu'\mu\mu'}^{r[11]}(-\tau), \quad (80)$$

so that it is sufficient to obtain explicitly only $\mathcal{K}^{r[11]}$. The non-diagonal terms are associated with complex ground state correlations, playing a relatively minor role in the gross features of the giant resonances. However, they may become important in quantifying fine spectral details, especially at low energies below the particle emission threshold, where the density of states is low.

Here I focus on $\mathcal{K}^{r[11]}$ as an example of how to proceed that can be applied to all components of the dynamical kernel. Its T -matrix reducible precursor

$$\mathcal{T}_{\mu\mu'\nu\nu'}^{r[11]}(t - t') = i \langle T[V, A_{\mu\mu'}](t) [V, A_{\nu\nu'}^\dagger](t') \rangle \quad (81)$$

is a time-ordered product of eight quasiparticle creation and destruction operators, four at time t and four at time t' . This constitutes a fully correlated two-times four-quasiparticle propagator contracted with two matrix elements of \bar{v} ; see Ref. [61] for details. Through this CF in the dynamical kernel, the two-fermion response

$\hat{\mathcal{R}}$ couples to EOMs for growing-rank CFs, similarly to the single-quasiparticle propagator, and again, various approximations may be generated by a cluster decomposition analogous to the one of Eq. (30):

$$\begin{aligned} G^{(4q)irr} \sim & G^{(q)} G^{(q)} G^{(q)} G^{(q)} + G^{(q)} G^{(q)} G^{(2q)} \\ & + G^{(2q)} G^{(2q)} + G^{(q)} G^{(3q)} + \sigma^{(4q)}, \end{aligned} \quad (82)$$

where the symbol $G^{(nq)}$ stands for any type of correlation functions with n quasiparticle operators. The qPVC approaches are associated with retaining the terms with at least one $G^{(2q)}$ which, by contraction with the pairs of interaction matrix elements, can be exactly mapped to the qPVC amplitudes as in Eqs. (35, 36, 58, 59).

Here, I narrow the discussion to the qPVC factorizations, which keep all the possible $G^{(2q)}$ contributions. As in the case of the single-fermion self-energy, the terms with $G^{(q)} G^{(q)}$ are partly absorbed in the $G^{(2q)}$ CFs, while their remaining contributions should be small in the leading-order qPVC at strong coupling. They can be evaluated afterward if better accuracy is sought. The leading contribution to $\mathcal{K}^{r[11]}$ takes the form [61]:

$$\begin{aligned} \mathcal{K}_{\mu\mu'\nu\nu'}^{r[11]cc}(\omega) = & \sum_{\gamma\delta nm} \left[\frac{\Gamma_{\mu\gamma}^{(11)n} \mathcal{X}_{\mu'\gamma}^m \mathcal{X}_{\nu'\delta}^{m*} \Gamma_{\nu\delta}^{(11)n*}}{\omega - \omega_{nm} + i\delta} \right. \\ & \left. - \frac{\Gamma_{\gamma\mu}^{(11)n*} \mathcal{Y}_{\mu'\gamma}^{m*} \mathcal{Y}_{\nu'\delta}^m \Gamma_{\delta\nu}^{(11)n}}{\omega + \omega_{nm} - i\delta} \right] - \mathcal{AS}, \end{aligned} \quad (83)$$

where $\omega_{nm} = \omega_n + \omega_m$ and \mathcal{AS} stands for antisymmetrizations, and the upper index "cc" indicates the approximation retaining CFs up to $G^{(2q)} G^{(2q)}$. The top line of Fig. 5 gives the diagrammatic interpretation of Eq. (83). The two-quasiparticle CFs figuring in the dynamical kernel (83) in the form of $\{\mathcal{X}, \mathcal{Y}\}$ components and frequencies ω_{nm} are formally exact and, thus, are not associated with any particular approximations, such as perturbative expansions or partial resummations. A remarkable consequence of this observation is that the cluster approaches retaining $G^{(2q)}$ CFs can include arbitrarily complex 2n-quasiparticle configurations non-perturbatively, which can be generated, e.g., iteratively in a self-consistent cycle. On the other hand, certainly, various approximations can be applied to calculations of these CFs and associated phonon characteristics.

As in the non-superfluid case, only one of the two two-fermion CFs can form a phonon, because only two matrix elements of the NN interaction are present in Eq. (76). Because of that, only one CF contracted with these matrix elements can be mapped to the qPVC. The correlations in the other two-fermion CF of Eq. (83), which is not associated with a phonon but rather forms an intermediate propagator (rectangular block in Fig. 5), can be relaxed, that leads to the qPVC-NFT approximation:

$$\mathcal{K}_{\mu\mu'\nu\nu'}^{r[11]c}(\omega) = \left\{ \left[\delta_{\mu'\nu'} \sum_{\gamma n} \frac{\Gamma_{\mu\gamma}^{(11)n} \Gamma_{\nu\gamma}^{(11)n*}}{\omega - \omega_n - E_{\mu'} - E_{\nu'}} \right. \right.$$

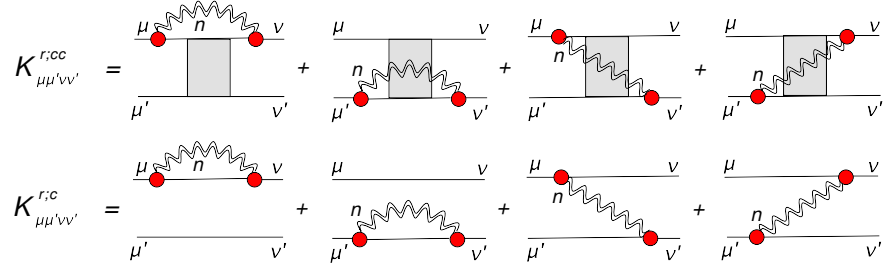


FIG. 5. The superfluid dynamical two-fermion kernels in the qPVC approximation. The complete multicomponent two-quasiparticle correlation function (69) is denoted by the shaded rectangular block. Top: the kernel of Eq. (83) with two two-quasiparticle correlation functions; bottom: the kernel of Eq. (85) with one two-quasiparticle correlation function, or leading-order qPVC.

$$-\sum_n \frac{\Gamma_{\mu\nu'}^{(11)n} \Gamma_{\nu\mu'}^{(11)n*}}{\omega - \omega_n - E_{\mu'} - E_{\nu'}} - [\mu \leftrightarrow \mu'] - \{\nu \leftrightarrow \nu'\}. \quad (84)$$

The index "c" marking this version of the dynamical kernel signals that only one two-quasiparticle CF is retained. Eq. (84) can be further transformed to the form recognizable as a superfluid generalization of the NFT's dynamical kernel by rearranging the antisymmetrizations as follows:

$$\begin{aligned} \mathcal{K}_{\mu\mu'\nu\nu'}^{r[11]c}(\omega) = & \left[\delta_{\mu'\nu'} \sum_{\gamma n} \frac{\Gamma_{\mu'\gamma}^{(11)n} \Gamma_{\nu\gamma}^{(11)n*}}{\omega - \omega_n - E_{\mu'\gamma}} + \delta_{\mu\nu} \sum_{\gamma n} \frac{\Gamma_{\mu'\gamma}^{(11)n} \Gamma_{\nu'\gamma}^{(11)n*}}{\omega - \omega_n - E_{\mu\gamma}} \right. \\ & \left. + \sum_n \frac{\Gamma_{\mu\nu}^{(11)n} \Gamma_{\nu'\mu'}^{(11)n*}}{\omega - \omega_n - E_{\mu'\nu}} + \sum_n \frac{\Gamma_{\mu'\nu'}^{(11)n} \Gamma_{\nu\mu}^{(11)n*}}{\omega - \omega_n - E_{\mu\nu'}} \right] \\ & - [\nu \leftrightarrow \nu']. \quad (85) \end{aligned}$$

If the pairing correlations are described by the BCS approximation, the dynamical kernels (83, 85) have the same form, but the quasiparticle energies E_μ and qPVC vertex functions $\Gamma_{\mu\nu}^{(ij)n}$ are replaced by their BCS analogs, where the U, V matrices are diagonal [115]. The resulting kernel is essentially an analog of the resonant kernels of the NFT [67] and quasiparticle time blocking approximation [36, 52] with qPVC introduced via the second-order perturbation theory. As mentioned above, a number of correlations were neglected in Eqs. (83, 85), which are considered to be the leading (resonant) approximations.

E. qPVC approaches for nuclear response in a relativistic self-consistent framework

Nuclear response beyond QRPA with the resonant qPVC dynamical kernel $\mathcal{K}^{r[11]c}$ has been a subject of self-consistent implementations with effective in-medium NN interactions derived from various versions of DFT.

The zero-range Skyrme interaction was employed, e.g., in Refs. [44, 67, 116, 117], and the QRPA+qPVC based on the relativistic meson-exchange interaction has been available since Ref. [41]. The latter method was formulated analytically in terms of the relativistic time blocking approximation (RQTBA) starting from the Bethe-Salpeter equation for the four-time two-quasiparticle propagator with phenomenologically inputted qPVC, following its original non-relativistic version [35, 36, 52]. The resonant superfluid dynamical kernels of Refs. [36, 41, 52] are consistent with the kernel of Eq. (85) in the BCS limit. However, we note that the time blocking and the necessity of the phenomenological qPVC can be ruled out in the ab initio theory discussed here. RQTBA demonstrated good performance in the more general context of the relativistic nuclear field theory (RNFT) including calculations for both the neutral [42, 45, 118–125] and charge-exchange [70, 71, 126, 127] excitations describing a large variety of nuclear phenomena with the same parameter set.

In the RNFT framework, significant improvements with respect to QRPA, due to the inclusion of the qPVC dynamical kernel have been found already in the leading approximation (85). The widths of the neutral giant resonances, Gamow-Teller and spin-dipole resonances, beta decay, nuclear compressibility, and other nuclear structure properties were described in a single framework with universal parameters across the nuclear chart. The self-consistency put stringent constraints on the calculation schemes via (i) approximating the static kernels of the one-fermion and two-fermion EOMs by the first and second variational derivatives of the energy density functional, respectively, (ii) obtaining the phonon characteristics with the same static kernels, and (iii) the subtraction of the static limit of the dynamical kernel [39] to eliminate the double counting of qPVC contained implicitly in the effective interaction. The complete self-consistency, the covariance of RNFT, and its rooting in particle physics provide a good balance of fundamentality, feasibility, and accuracy. The theory appears as predictive, transferrable across the energy scales, and systematically improvable due to the variability of the dynamical kernel and its or-

ganization in accordance with the qPVC power counting. The latter two features were enabled after the completion of the ab initio EOM qPVC framework [17, 26, 46, 61] outlined in these lectures. Further effort allowed a formulation of RNFT for finite temperatures [128–131] extending its applications to astrophysically relevant phenomena.

III. NUCLEAR RESPONSE IN THE RNFT FRAMEWORK

A. Electromagnetic response

The electromagnetic response is the most studied type of nuclear response as it can be induced by the most accessible experimental probes with photons [132–134]. The corresponding excitation operators are classified by the transferred angular momentum L and parity π [133]. The electric operators have natural parity, i.e., $\pi = (-1)^L$, and are defined as

$$\begin{aligned} F_{00} &= e \sum_{i=1}^Z r_i^2, \\ F_{1M} &= \frac{eN}{A} \sum_{i=1}^Z r_i Y_{1M}(\hat{\mathbf{r}}_i) - \frac{eZ}{A} \sum_{i=1}^N r_i Y_{1M}(\hat{\mathbf{r}}_i), \\ F_{LM} &= e \sum_{i=1}^Z r_i^L Y_{LM}(\hat{\mathbf{r}}_i), \quad L \geq 2, \end{aligned} \quad (86)$$

where e stands for the proton charge, $Y_{LM}(\hat{\mathbf{r}})$ are the spherical harmonics, and Z and N are the numbers of protons and neutrons in a nucleus, respectively. The expression for $L = 1$ contains the “kinematic” charges to account for the center-of-mass motion. Otherwise, the electric excitation operators (86) imply only the interaction of the projectiles with the charged protons and no interaction with the neutrons. The corresponding isoscalar operators with zero isospin transfer contain summations over all the nucleons and no electric charge, if they are not associated with the electric probes. The isoscalar dipole operator reads

$$F_{1M}^{(0)} = \sum_{i=1}^A (r_i^3 - \eta r_i) Y_{1M}(\hat{\mathbf{r}}_i), \quad (87)$$

where $\eta = 5\langle r^2 \rangle / 3$, and the second term in the brackets eliminates the spurious translational mode [135]. The superscript ‘(0)’ indicates the isoscalar character of the operator, $\Delta T = 0$, in contrast to the operators (86), which are often classified as isovector ones with $\Delta T = 1$. The magnetic multipole operators are of the unnatural parity $\pi = (-1)^{L+1}$ and of a more complex nature. Magnetic resonances are associated with spin transfer and, generally, do not exhibit pronounced collectivity [136]. While magnetic transitions will be discussed elsewhere, I will focus on the electric dipole transitions in this subsection.

The response of strongly correlated systems to external perturbations manifests some generic features of the excitation spectra, which can be captured by a schematic model proposed by Brown and Bolsterli [101, 137]. In this model, which adopts a separable effective multipole-multipole interaction, the RPA excitation spectrum contains two highly collective states, the low-frequency and the high-frequency ones. These two states are formed by the coherent particle-hole contributions from the uncorrelated ph -excitations (with respect to the Hartree-Fock or the phenomenological mean-field vacuum), when the interaction is switched on. The remaining ph states are mostly non-collective and lie between the two collective solutions. In the RPA calculations with more realistic interactions, the resulting spectrum depends on the nature of the residual interaction and on the quality of the numerical implementation. The general gross structure of the spectrum remains as in the Brown-Bolsterli model, but the main collective solutions undergo some fragmentation, the so-called Landau damping. Typically, the low-energy solutions are not very collective in the $L = 0$ and $L = 1$ channels, but acquire collectivity at larger angular momentum transfer $L \geq 2$. The high-energy ones are associated with collective oscillations, which involve all the nucleons. Taking into account the dynamical kernel, in any of the approximations discussed above, induces further fragmentation of the ph states due to their coupling to more complex configurations. This effect is a consequence of the pole structure of the dynamical kernel. The fine details of the obtained spectra vary depending on the approximation to $K^{(r)}$.

Figure 6 shows the cross sections of the total dipole photoabsorption in four medium-mass spherical nuclei obtained within the relativistic QRPA (RQRPA) [140] (black dashed curves) and RQTBA [41] (red solid curves), compared with the neutron data (blue error bars) from Ref. [141]. This cross section is defined as

$$\sigma_{E1}(E) = \frac{16\pi^3 e^2}{9\hbar c} E S_{E1}(E), \quad (88)$$

i.e., with the additional energy factor in front of the strength distribution, which slightly emphasizes the high-energy part of the nuclear response. The RQTBA calculations employ the qPVC dynamical kernel in its NFT form (85). The in-medium interaction is of the effective meson-exchange origin and adjusted to bulk nuclear properties in the framework of the covariant DFT [112, 139, 142] with the NL3 parametrization [110]. In the fully self-consistent calculation scheme, the RQRPA generally produces the dipole strength, which is mostly concentrated in a narrow energy region. The localization of the centroid is reproduced fairly well, as compared with the data, however, the observed strength exhibits a broad and relatively smooth peak called giant dipole resonance (GDR) [132].

The total transition probability is another characteristic of the GDR, which is typically reproduced also well in the (Q)RPA approaches. The most robust related quan-

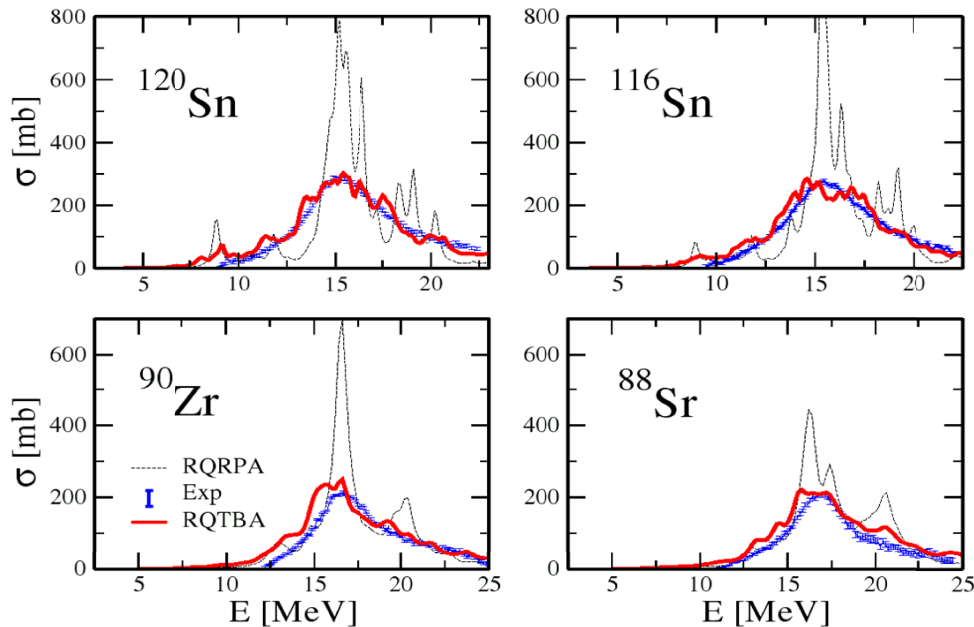


FIG. 6. Total dipole photoabsorption cross section in stable medium-mass nuclei. The figure is adopted from Refs. [138, 139].

tity is the energy-weighted sum rule (EWSR),

$$S_{E1} = \sum_{\nu} E_{\nu} B_{\nu} = \frac{9\hbar^2 e^2}{8m_p} \frac{NZ}{A}, \quad (89)$$

which is proportional to the cross section integrated over the energy variable, and B_{ν} are the squared transition matrix elements appearing in Eq. (64). The right hand side of Eq. (89) is calculated by transforming the sum into a double commutator of the dipole excitation operator and the system Hamiltonian, under the assumption that the interaction between nucleons has no momentum dependence. In this case, the potential energy part commutes with the excitation operator and, thus, does not contribute to the sum rule [101]. The relation (89) is, therefore, valid for any Hamiltonian without momentum dependence in the two-body sector and known as Thomas-Reiche-Kuhn sum rule. Modern energy density functionals (EDFs), such as the Skyrme, Gogny, and relativistic ones yield the effective interactions, which depend on the nucleonic momenta, so that a 10–20% or even larger enhancement of the dipole EWSR can be obtained in the (Q)RPA calculations [143], in agreement with experiments, where the measurements span sufficiently broad energy intervals [141].

Adding the dynamical kernels, which satisfy the consistency conditions between the self-energy and the exchange terms, should not violate the EWSR [52]. In particular, the resonant qPVC kernels of the NFT form satisfy this condition. Thus, the EWSR conservation serves as a very good test for numerical implementations. The subtraction procedure [39], which is applied to eliminate the double counting of the qPVC effects in EDFs, in-

duces a slight violation of the EWSR, because it modifies the static part of the interaction kernel and pushes the centroid upward, but the resulting position of the major peak is rather close to its (Q)RPA placement. Otherwise, the dynamical kernel alone shifts the major peak to lower energy. This is a desirable feature in the *ab-initio* implementations, such as the second RPA studied in Ref. [144]. However, if a reasonable effective interaction is employed for the dynamical kernel, the major peak is already well positioned in (Q)RPA, so that its downward shift by the dynamical kernel is well compensated by the subtraction. This procedure is quite simple and consists of the replacement,

$$\begin{aligned} \tilde{\mathcal{K}}^0 + \tilde{\mathcal{K}}^r(\omega) &\rightarrow \tilde{\mathcal{K}}^0 + \delta\tilde{\mathcal{K}}^r(\omega) \\ &= \tilde{\mathcal{K}}^0 + \tilde{\mathcal{K}}^r(\omega) - \tilde{\mathcal{K}}^r(0), \end{aligned} \quad (90)$$

i.e., the dynamical kernel in the static approximation $\omega = 0$ is subtracted from the dynamical kernel itself. The energy-independent combination $\tilde{\mathcal{K}}^0 - \tilde{\mathcal{K}}^r(0)$, thus, stands for the effective interaction freed from the long-range effects taken into account by $\tilde{\mathcal{K}}^r(\omega)$. The ‘ \sim ’ sign in Eq. (90) marks the kernels, where the effective interaction is employed, that is, the entire static kernel $\tilde{\mathcal{K}}^0$ and the interaction matrix elements in the topologically equivalent dynamical kernels $\tilde{\mathcal{K}}^r(\omega)$ computed in various approximations.

One can further see from Figure 6, that the coupling between the superfluid quasiparticles and phonons included within RQTBA provides a sizable fragmentation and broadening of the GDR. Due to the inclusion of a large number of the phonon modes, the final strength distribution acquires nearly a Lorentzian shape,

though relatively small values of the smearing parameter, $\Delta = 200$ keV for the Sn isotopes and $\Delta = 400$ keV for Sr and Zr, were used in both the RQRPA and RQTBA calculations. The choice of these parameters was based on the estimate of the continuum contribution, which was not included explicitly.

In principle, the particle escape to the continuum plays a role in the formation of the width of the high-frequency resonances above the particle emission threshold. The latter is the minimal energy, at which the nucleon emission is possible, often called nucleon binding, or separation, energy, and its typical value is ~ 7 – 10 MeV for stable medium-mass and heavy nuclei. Loosely-bound exotic nuclei with strong dominance of one type of nucleons (protons or neutrons) are characterized by lower separation energies for the excess nucleons. For example, in neutron-rich nuclei, neutrons are loosely bound and have lower separation energy than protons, and vice versa. The effect of the single-particle continuum in the (Q)RPA and beyond-(Q)RPA calculations can be taken into account within the method first proposed in Ref. [145] for RPA, later extended to QRPA [146–151] and QRPA+qPVC [36]. The complete inclusion of the single-particle continuum in these methods is achieved by employing the coordinate-space representation for the (Q)RPA propagator and the final EOM, while the qPVC part of the propagator in Ref. [36] is transformed to the coordinate space via the single-particle wave functions. In Ref. [146], a modification of this method was proposed for the numerical solution of the response EOM in the discrete basis of the single-particle states with the box boundary condition. Both the original and modified methods are based on constructing the mean-field propagator from the regular and irregular single-particle wave functions as the mean-field solutions with the Coulomb or free asymptotics.

The single-particle continuum does not play a quantitatively important role in the description of highly excited states of well-bound medium-mass and heavy nuclei, producing a typical continuum width of the order of 100 keV for every single peak in the spectrum above the particle threshold, although the role of continuum increases dramatically in light nuclei, especially the loosely bound ones. Clear examples are given in Ref. [146]. The inclusion of multiparticle continuum in the (Q)RPA extensions was not addressed in the nuclear physics literature until now, though effects of two-nucleon evaporation should become sensible already at the GDR centroid energy and further escape of more nucleons can affect the GDR's high-energy shoulder.

Comprehensive calculations for the nuclear response of various non-spin-flip multipoles with Skyrme interaction and basic qPVC dynamical kernels can be found, for instance, in Refs. [146]. Overall, the models with various types of dynamical kernels confined by correlated or non-correlated $2p2h$ configurations, although quite successful, still have not reached the spectroscopic accuracy of even hundreds of keV in the description of excitation spectra

and other properties of medium-mass and heavy nuclei, which can be associated with these spectra. Despite the convincing progress on both the beyond-(Q)RPA methods and the EDFs, it remains unclear to what degree the lack of accuracy should be attributed to the imperfections of the EDFs, truncations in the beyond-(Q)RPA calculation schemes, unavoidable with the present computational capabilities, or principal limitations of these many-body methods. Up until now, the majority of nuclear response calculations beyond (Q)RPA include up to the (correlated) $2p2h$ configurations [41, 42, 66, 69–71]. Calculations with the $3p3h$ configuration complexity [17, 18, 80–82, 84, 85] are much more difficult but gradually become available. Direct comparison between the $2p2h$ and $3p3h$ calculations within the same implementation schemes indicates that the latter higher-rank configurations (i) improve the results noticeably and (ii) the effect of the inclusion of $3p3h$ configurations, in addition to $2p2h$ ones, is weaker than the effect of the inclusion of $2p2h$ configurations beyond (Q)RPA. The former points to the importance of the $3p3h$ configurations, and the latter means that the theory exhibits saturation with respect to the configuration complexity.

An example is given in Fig. 7, where $3p3h$ configurations were included in the "two quasiparticles coupled to two phonons" ($2q \otimes 2phonon$) scheme for the electromagnetic dipole response of $^{68,70}\text{Ni}$. This was achieved by implementing the dynamical qPVC kernel in an iterative cycle. Namely, after computing and selecting the most relevant RQRPA phonon modes (by solving BSDE without dynamical kernels), the $2q \otimes phonon$ dynamical kernel was constructed, and the response was calculated with this kernel for the most relevant J^π ($J \leq 6$) channels of both parities. After that, the obtained response functions were recycled in the dynamical kernel of the EOM for the dipole response. This scheme was originally proposed in Ref. [153] as an extension of the quasiparticle time blocking approximation, and later re-derived starting from the bare Hamiltonian. The approach is dubbed here as REOM³ due to its construction. The electromagnetic dipole strength functions obtained within REOM³ (red solid curves) are plotted in Fig. 7 together with the results of RQRPA (black dot-dashed curves), REOM² (RQTBA) (blue dashed curves) and experimental data (error bars) of Ref. [152].

The GDR in medium-light calcium isotopes was investigated within the RQTBA framework in Ref. [124] with the focus on the role of the $2q \otimes phonon$ configurations in the width of the GDR. It was found that these configurations result in the formation of the spreading width and significantly improve the agreement to data as compared to RQRPA. Nevertheless, although the authors used a large model space of the $2q \otimes phonon$ configurations with the RQRPA phonons, the total width of the GDR was still underestimated. In addition, on the high-energy shoulder of the GDR the cross sections were found systematically lower than the experimental ones. A similar situation was reported in Ref. [146], for

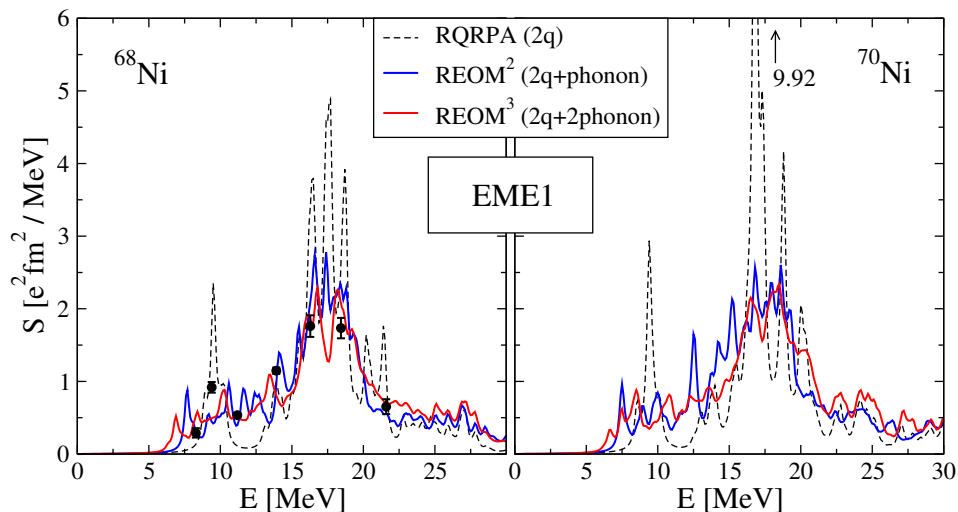


FIG. 7. Giant dipole resonance in $^{68,70}\text{Ni}$ calculated within the RQRPA and REOM $^{(2,3)}$ approaches [17], in comparison with the experimental data [152]. The figure is adopted from Ref. [18].

QTBA calculations with various Skyrme forces. These observations pointed out that further refinement of the dynamical kernels may be necessary. Taking into account more complex $2q \otimes 2\text{phonon}$ configurations in Ref. [17] indicated that these problems can be potentially resolved for medium-light nuclei by this method. Fig. 7 further validates this assumption for the neutron-rich nickel isotopes. Although the experimental data are of low energy resolution and available only for ^{68}Ni , one can see that the new higher-rank configurations in REOM 3 cause additional fragmentation of the GDR and, thus, intensify the spreading of the strength to both higher and lower energies. Technically, this is the consequence of the appearance of the new poles in the resulting response function. These new poles rearrange the energy balance of the strength distribution in both the low-energy and the higher-energy sectors, however, without violating the dipole EWSR [17].

Response of non-spherical nuclei to external probes, in general, is more difficult to calculate microscopically. Already on the QRPA level, the $2q$ model space expands dramatically, as compared to the spherical case. The reason is the lifted degeneracy of j -orbitals, because the total angular momentum is not a good quantum number in non-spherical geometries. Therefore, even QRPA calculations are numerically very expensive already in axially deformed nuclei [154]. In particular, such calculations require numerical evaluation of the enormous amount of matrix elements of the nucleon-nucleon interaction, which makes deformed QRPA prohibitively difficult even in the DFT frameworks. See also Refs. [155, 156] for the studies along this direction. An elegant numerical solution was proposed in Ref. [157], where the finite-amplitude method (FAM), avoiding direct computation of the interaction matrix elements, was developed and employed for RPA calculations of the response of de-

formed nuclei. Later on, the FAM-RPA was generalized to superfluid nuclei as FAM-QRPA [158–160].

Recently available formulations of the qPVC in the HFB basis [46, 61] allowed to generalize FAM-QRPA to FAM-qPVC, with the numerical implementation in the axially deformed bases for one-fermion [109] and two-fermion [161] EOMs. These calculations in the leading-order qPVC show good performance in the description of the single-quasiparticle states and Gamow-Teller strength distributions, respectively. Alternatively, the description of moderately deformed nuclei can be performed in a spherical basis by generating configurations of higher complexity; see, for instance, Ref. [85], where the dipole response of the deformed ^{64}Ni was computed in REOM 3 . This is technically possible when the low-lying phonons are accessible by spherical QRPA without encountering the instabilities associated with the deformed phase transition. In this case, the self-consistently generated complex configurations induce the proper spatial arrangement of strongly-coupled nucleons dynamically, instead of the static deformation imposed by the mean-field basis.

B. Spin-isospin response

The nuclear spin-isospin response, also known as the charge-exchange excitations, corresponds to the transitions from the ground-state of the nucleus (N, Z) to the final states in the neighboring nuclei ($N \mp 1, Z \pm 1$) in the isospin lowering T_- and raising T_+ channels, respectively. These excitations can take place spontaneously, e.g., in the famous β decays, or be induced by external fields, e.g., in the charge-exchange reactions, such as (p, n) or ($^3\text{He}, t$). Nuclear spin-isospin responses are categorized into different modes according to the nucleons

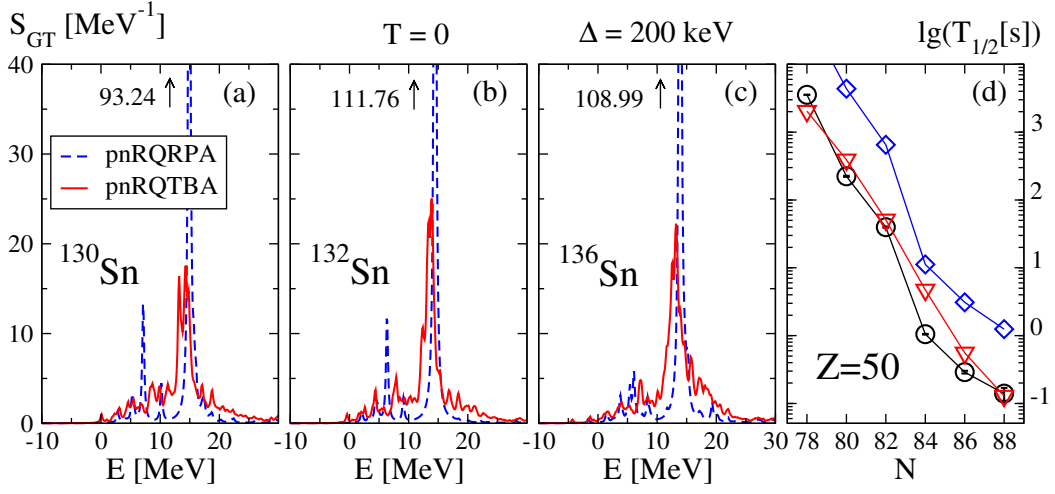


FIG. 8. GT₋ strength distribution for ^{130,132,136}Sn nuclei at zero temperature in the pnRQTBA, compared to the pnRQRPA (a-c). Beta decay half-lives in neutron-rich tin isotopes extracted from the pnRQRPA (diamonds) and pnRQTBA (triangles) strength distributions, compared to data (circles) [141] (d). The figure is adopted from Ref. [130].

with spin-up and spin-down oscillating either in phase, the non-spin-flip modes with $S = 0$, or out of phase, the spin-flip modes with $S = 1$. The important modes, which have attracted an extensive attention experimentally and theoretically, include the isobaric analog state with $S = 0$, $J^\pi = 0^+$, Gamow-Teller resonance (GTR) with $S = 1$, $J^\pi = 1^+$, and spin-dipole resonance with $S = 1$, $J^\pi = 0^-, 1^-, 2^-$ [162–165].

The corresponding operators of these charge-exchange excitations read

$$\begin{aligned}
 F_{IAS}^\pm &= \sum_{i=1}^A \tau_\pm(i), \\
 F_{GTR}^\pm &= \sum_{i=1}^A [1 \otimes \vec{\sigma}(i)]_{J=1} \tau_\pm(i), \\
 F_{SDR}^\pm &= \sum_{i=1}^A [r_i Y_1(i) \otimes \vec{\sigma}(i)]_{J=(0,1,2)} \tau_\pm(i), \quad (91)
 \end{aligned}$$

where σ and τ are the Pauli matrices of spin and isospin degrees of freedom, respectively. The corresponding non-energy-weighted sum rules (NEWSR), $S^- - S^+ = \sum_\nu B_\nu^- - \sum_\nu B_\nu^+$, are

$$\begin{aligned}
 S_{IAS}^- - S_{IAS}^+ &= N - Z, \\
 S_{GTR}^- - S_{GTR}^+ &= 3(N - Z), \\
 S_{SDR}^- - S_{SDR}^+ &= \frac{9}{4\pi} [N \langle r^2 \rangle_n - Z \langle r^2 \rangle_p], \quad (92)
 \end{aligned}$$

where the GTR one is the famous model-independent Ikeda sum rule, while the SDR one involves the root-mean-square radii of protons and neutrons and is considered to be an alternative way for measuring neutron skin thickness [166, 167]. For neutron-rich nuclei, the excitations in the T_+ channel are significantly suppressed

by the Pauli principle, and thus S^- alone approximately represents the NEWSR.

The GTR, which is the most studied nuclear spin-isospin response, is related to both the spin-orbit and isospin properties of nuclear systems. Although this relationship is not direct and clouded by complex many-body correlations, experimental data on the GTR can be used to constrain the respective terms in the effective interactions and EDFs. For instance, one of the recently developed and widely used Skyrme effective interactions, SAMi [168], has acquired improved spin-isospin properties by providing an accurate description of GTR peak energies. In the relativistic framework, it was found that on the (Q)RPA level an accurate description of GTR peak energies can be achieved in a fully self-consistent way by taking the Fock terms of the meson-exchange interactions into account [169–171].

Overall, RPA and QRPA with effective interactions [169–174] produce reasonable results for the major GTR peak. However, reproducing the detailed strength distribution is impossible within these approaches neglecting the dynamical correlations. Moreover, since the total strength is constrained by the model-independent Ikeda sum rule, it is exhausted within the relatively narrow energy interval, because of the model space limitations of (Q)RPA. This causes, to a large extent, the well-known quenching problem [162]. The overall situation is similar to that with electromagnetic excitations, and the GTR is considerably affected by the effects beyond (Q)RPA. While SRPA calculations for the GTR have been reported already in 1990 [175], calculations with the qPVC kernels based on modern density functionals, both relativistic NL3 [70, 71, 127, 176] and non-relativistic Skyrme [66], have become available more recently. Lately, SRPA calculations were also performed with the Skyrme interaction [177]. Despite technical differences between

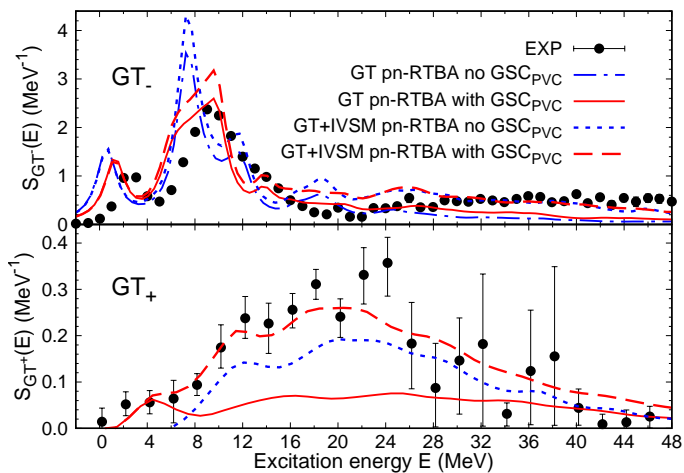


FIG. 9. GT strength distributions for the transitions $^{90}\text{Zr} \rightarrow ^{90}\text{Nb}$ (top) and $^{90}\text{Zr} \rightarrow ^{90}\text{Y}$ (bottom). The pure GT strength and the mixed GT+IVSM strength of pnRTBA without GSC_{PVC} (dashed-dotted and dotted blue) and with GSC_{PVC} (solid and dashed red) are displayed, in comparison to the experimental data [179, 180]. The figure is adopted from Ref. [71].

the various implementations, all the extensions beyond (Q)RPA improve the description of the GTR considerably. In the cases of neutron-rich nuclei, where the low-energy part of the GTR spectrum is associated with spontaneous beta decay, the description of beta decay rates are improved by up to one or two orders of magnitude, compared to those obtained in (Q)RPA [70, 130].

The role of the qPVC effects is illustrated in Fig. 8 for the response of the neutron-rich tin isotopes $^{130,132,136}\text{Sn}$ to the GT_- operator, obtained within the proton-neutron version of RQTBA (pnRQTBA) with the qPVC dynamical kernel, which was originally developed in Ref. [70]. These calculations are compared to the proton-neutron RQRPA (pnRQRPA) without the dynamical kernel, and the presented spectra are displayed on the energy scales relative to the parent nuclei. The most general observation from these calculations is that qPVC leads to a similar degree of fragmentation as in non-charge-exchange channels, which is somewhat higher in nuclei with larger isospin asymmetry. In turn, this fragmentation redistributes the strength in the low-energy sector, in particular, in the Q_β energy window. This leads to faster beta decay in the pnRQTBA calculations, improving significantly the agreement with experimental data [141], as compared to pnRQRPA. The corresponding half-lives are shown in the right panel of Fig. 8. More examples, details, and discussions of GTR calculations within pnR(Q)RPA are presented in Ref. [70, 178], while SDR calculations were reported in Ref. [176]. Furthermore, the pnRTBA has been generalized recently to finite temperature, which allows applications to beta decay and electron capture in stellar environments [130, 131].

The most advanced calculations with the PVC kernel included, in addition to the standard NFT terms, also the ground state correlations (GSC) caused by PVC (GSC_{PVC}). These correlations were introduced and discussed in detail, for instance, in Refs. [34, 181], where their role in the spin-flip magnetic dipole excitations was found significant. As the GTR also involves the spin-flip process, an important contribution from the GSC_{PVC} is expected. It can be especially significant in the GT_+ branch in neutron-rich nuclei, where these correlations were found to be solely responsible for the unblocking mechanism [71]. An example is given in Fig. 9, where the GT_\pm strength distributions in ^{90}Zr are shown in comparison to data of Refs. [179, 180]. In the GT_- branch of the response, the inclusion of the PVC effects within the pnRTBA leads to an overall fragmentation and broadening of the strength distribution, as compared to the pnRRPA (not shown). In the GT_+ branch, in principle, the GSC of RPA (GSC_{RPA}) can unlock transitions from particle to hole states, but such transitions appear only above 7 MeV with very low probabilities. The inclusion of PVC in the pnRTBA with only the leading resonant NFT forward-going diagrams in the PVC kernel induces almost no change. However, the inclusion of the GSC_{PVC} associated with backward-going PVC processes has a very strong effect on the GT_+ strength. These correlations cause fractional occupancies of the single-particle states of the parent nucleus, which unlocks new transitions between the states on the same side of the Fermi surface. For instance, the peak around 4.5 MeV appears mainly due to the $\pi 1g_{9/2} \rightarrow \nu 1g_{7/2}$ and $\pi 2p_{3/2} \rightarrow \nu 2p_{1/2}$ transitions, with the sizeable absolute values of the transition densities of 0.347 and 0.182, respectively.

In the calculations shown in Fig. 9, the theoretical GT_+ and GT_- strength distributions were smeared with a parameter $\Delta = 2$ and 1 MeV, respectively, to match the experimental energy resolutions. As in the case of electromagnetic excitations, the pnRRPA calculations do not provide a good agreement with data; therefore, they are not shown. In the GT_- channel, the pnRTBA with GSC_{PVC} demonstrates a good agreement with the data up to ~ 25 MeV, except for a small mismatch of the position of the low-lying state. Remarkably, in the GT_+ channel, the GSC induced by PVC are solely responsible for the appearance of both the low-energy peak at 4 MeV and the higher-energy strength up to ~ 50 MeV. Above the low-lying peak, even the pnRTBA GT_+ strength alone largely underestimates the data. It is well known, however, that at large excitation energy contributions of the isovector spin-monopole (IVSM) mode become important. The data of Refs. [179, 180], in particular, also contain the contribution of the IVSM excitations, which could not be disentangled from the GT transitions due to technical difficulties. The IVSM modes are generated by the response to the operator $F_{IVSM}^\pm = \sum_i r^2(i) \vec{\Sigma}(i) \tau_\pm(i)$, which should be mixed with the GT response, for instance, following the procedure of Ref. [182]. It introduces the mixed

operator $F_{\alpha}^{\pm} = \sum_i [1 + \alpha r^2(i)] \vec{\Sigma}(i) \tau_{\pm}(i)$, where α is a parameter adjusted to reproduce the magnitude of the theoretical low-energy GT strength. In this way, the values $\alpha = 9.1 \times 10^{-3}$ and $\alpha = 7.5 \times 10^{-3} \text{ fm}^{-2}$ were adopted for the GT_+ and GT_- branches, respectively. After that, as one can see from Fig. 9, the resulting strength above 25-30 MeV reasonably describes the data in the (p,n) branch, thus highlighting the importance of both the GSC_{PVC} and the IVSM contribution. In the (n,p) channel the results are also improved after adding the GSC_{PVC} and the IVSM in pnRTBA, so that a very good agreement of the overall strength distribution is obtained also for GT_- . Further details and discussions of this case can be found in Ref. [71].

IV. SUMMARY AND OUTLOOK

In these lectures, I discussed fermionic in-medium equations of motion and their applications to nuclear structure with a major focus on the nuclear response. We have seen that the EOM for the two-quasiparticle propagator provides a formally complete theory to describe nuclear spectra, however, it admits only approximate solutions. Starting from the most general many-body Hamiltonian, we constructed a model-independent theoretical framework for the lowest-rank in-medium fermionic propagators. Approximations, most relevant in the intermediate and strong coupling regimes, to the commonly accessible observables are derived and discussed. The new scale with the order parameter associated with emergent collective degrees of freedom was used to advance the dynamical interaction kernels in a systematically improvable way.

The EOM for the one-fermion propagator is worked out in a single-particle basis, first in the absence of superfluidity. Subsequently, we added superfluid pairing correlations and transformed the single-particle sector of the theory to the HFB basis, relaxing the particle number constraint. This representation enabled scaling the computational effort down considerably and paved the way for the superfluid response theory, which was built in the HFB basis from the start. In particular, the unification of particles and holes in the quasiparticle concept established the framework to unify the particle-hole and particle-particle channels in the response theory. The dynamical interaction kernels appearing in the integral parts of the EOMs in terms of higher-rank propagators are discussed in detail as they represent the major obstacle to accurate solutions of the nuclear many-body problem. The latter propagators are approximated by factorizations into the possible products of CFs. For practical applications to nuclear structure, introducing a truncation of the many-body problem on the two-body level is possible by retaining two-fermion and one-fermion CFs. The presence of the two-body CFs is found to be the minimal requirement for keeping the leading effects of emergent collectivity. Then, we discussed how, by gradually

relaxing correlations, the theory with factorized dynamical kernels can be reduced to further approximations.

The practical inclusion of the quasiparticle-vibration coupling, or qPVC, in the dynamical kernels of the response theory is discussed in the context of numerical implementations for nuclear spectral calculations. Selected results are presented in the RNFT framework for the dipole and Gamow-Teller (GT) responses of medium-mass nuclei. The leading-order qPVC effects are shown to considerably modify the spectral strength distributions, obtained in the relativistic QRPA, causing fragmentation of the QRPA modes and shifting the positions of the major peaks. An example of a higher configuration complexity up to $2q \otimes 2\text{phonon}$ was considered for the electromagnetic dipole strength distribution in medium-light nuclei. Overall, the increase of configuration complexity brings the theoretical results in better agreement with the data [17, 86] and the resulting strength functions show saturation of its general features with the increase of configuration complexity. Another type of complex correlations, namely the qPVC-associated ground state correlations, was found to play a sizeable role in the nuclear response induced by weak interactions. The case of GT_+ response of a neutron-rich ^{90}Zr was brought up as an example of this kind.

Besides being an interesting theoretical problem, the response theory has many applications, where accurate nuclear excitation spectra are required, especially at the extremes of energy, mass, isospin, and temperature. The most prominent example is nuclear astrophysics, in particular, the rapid neutron capture process (*r*-process) nucleosynthesis in kilonova, core-collapse supernovae, and neutron star mergers [183]. The nuclear response to the electric and magnetic dipole, Gamow-Teller and spin-dipole operators are the microscopic sources of the major astrophysical reaction rates, such as the radiative neutron capture (n, γ), electron capture, β decay, and β -delayed neutron emission. These rates are very sensitive to the fine details of the calculated response, or strength functions, in the given channels, and needed for many nuclei, including those, which are not accessible in laboratory. The low-energy parts of the listed strength distributions are of particular importance. The low-lying dipole strength, which is relevant for the (n, γ) rates, was studied very intensively during the past decades and associated with the neutron skin oscillations. In the neutron-rich nuclei, lying on the *r*-process path in the nuclear landscape, such oscillations form the pygmy dipole resonance, which can affect the (n, γ) rates considerably [118, 134, 164, 184]. The low-energy parts of the GTR and SDR are responsible for the beta decay and electron capture rates [170, 185–187]. The recent developments have demonstrated, in particular, that the weak reaction rates are affected considerably by the nuclear correlations beyond QRPA [66, 70, 127, 130, 131, 170]. Nevertheless, the simplistic QRPA theoretical reaction rates, as well as the mean-field nuclear matter equation of state, are still employed in most astrophysical simulations, while

the deficiencies of these approaches are even more amplified in stellar environments [188–191]. Therefore, adopting the microscopic methods advanced beyond QRPA for astrophysical simulations is an important step toward a high-quality nuclear physics input for such simulations.

The inability of the theory to provide accurate nuclear spectra impedes the progress in other related applications, including the searches for new physics beyond the Standard Model in the nuclear domain, such as the neutrinoless double β decay and the electric dipole moment. These phenomena involve a delicate interplay of numerous emergent effects beyond the mean-field and QRPA and, thus, also require computation of consistency and accuracy, which are beyond the limits of current state-of-the-art theoretical and computational approaches to the nuclear response. The insufficient quality of their results accentuates the importance of further advancing

the quantum many-body theory in the sector of dynamical complex configurations, which, in turn, gives feedback on the static kernels of the fermionic EOMs. Therefore, a major hope to resolve the issues discussed above is to reconcile consistently the static and dynamical kernels of the two-fermion EOMs in various channels, based on the lessons learned from the approaches implemented up to date. This has to be complemented by a serious effort on refining nuclear interactions, both bare and effective interactions, desirably compatible with special relativity and rooted in particle physics.

ACKNOWLEDGEMENT

This work was supported by the GANIL Visitor Program, US-NSF Grant PHY-2209376, and US-NSF Career Grant PHY-1654379.

-
- [1] T. Matsubara, *Progress in Theoretical Physics* **14** (1955).
 - [2] K. M. Watson, *Physical Review* **103**, 489 (1956).
 - [3] K. A. Brueckner and C. A. Levinson, *Physical Review* **97**, 1344 (1955).
 - [4] K. A. Brueckner, *Physical Review* **100**, 36 (1955).
 - [5] P. C. Martin and J. S. Schwinger, *Physical Review* **115**, 1342 (1959).
 - [6] S. Ethofer, *Zeitschrift für Physik A* **225**, 353 (1969).
 - [7] P. Schuck and S. Ethofer, *Nuclear Physics* **A212**, 269 (1973).
 - [8] L. P. Gorkov, *Soviet Physics JETP* **7**, 505 (1958).
 - [9] L. P. Kadanoff and P. C. Martin, *Physical Review* **124**, 670 (1961).
 - [10] S. Ethofer and P. Schuck, *Zeitschrift für Physik* **228**, 264 (1969).
 - [11] A. Migdal, *Theory of finite Fermi systems and application to atomic nuclei* (Wiley-Interscience Publ., 1967).
 - [12] S. Adachi and P. Schuck, *Nuclear Physics* **A496**, 485 (1989).
 - [13] P. Danielewicz and P. Schuck, *Nuclear Physics* **A567**, 78 (1994).
 - [14] J. Dukelsky, G. Röpke, and P. Schuck, *Nuclear Physics* **A628**, 17 (1998).
 - [15] C. Popovici, P. Watson, and H. Reinhardt, *Physical Review D* **81**, 105011 (2010).
 - [16] C. Popovici, P. Watson, and H. Reinhardt, *Physical Review D* **83**, 025013 (2011).
 - [17] E. Litvinova and P. Schuck, *Physical Review C* **100**, 064320 (2019).
 - [18] E. Litvinova, *European Physical Journal A* **59**, 291 (2023).
 - [19] M. L. Tiago, P. Kent, R. Q. Hood, and F. A. Reboredo, *Journal of Chemical Physics* **129**, 084311 (2008).
 - [20] J. I. Martinez, J. García-Lastra, M. López, and J. Alonso, *Journal of Chemical Physics* **132**, 044314 (2010).
 - [21] D. Sangalli, P. Romaniello, G. Onida, and A. Marini, *Journal of Chemical Physics* **134**, 034115 (2011).
 - [22] P. Schuck and M. Tohyama, *European Physical Journal A* **52**, 307 (2016).
 - [23] V. Olevano, J. Toulouse, and P. Schuck, *Journal of Chemical Physics* **150**, 084112 (2018).
 - [24] P. Schuck, D. Delion, J. Dukelsky, M. Jemai, E. Litvinova, G. Röpke, and M. Tohyama, *Physics Reports* **929**, 1 (2021).
 - [25] P. Schuck, *European Physical Journal A* **55**, 250 (2019).
 - [26] E. Litvinova and P. Schuck, *Physical Review C* **102**, 034310 (2020).
 - [27] E. Litvinova and P. Schuck, *Physical Review C* **104**, 044330 (2021).
 - [28] A. Bohr and B. R. Mottelson, *Nuclear structure*, Vol. 1 (World Scientific, 1969).
 - [29] A. Bohr and B. R. Mottelson, *Nuclear structure*, Vol. 2 (Benjamin, New York, 1975).
 - [30] R. A. Broglia and P. F. Bortignon, *Physics Letters* **B65**, 221 (1976).
 - [31] P. F. Bortignon, R. Broglia, D. Bes, and R. Liotta, *Physics Reports* **30**, 305 (1977).
 - [32] G. Bertsch, P. Bortignon, and R. Broglia, *Reviews of Modern Physics* **55**, 287 (1983).
 - [33] F. Barranco, G. Potel, R. A. Broglia, and E. Vigezzi, *Physical Review Letters* **119**, 082501 (2017).
 - [34] S. Kamenzhiev, J. Speth, and G. Tertychny, *Physics Reports* **393**, 1 (2004).
 - [35] V. Tselyaev, *Soviet Journal of Nuclear Physics* **50**, 780 (1989).
 - [36] E. Litvinova and V. Tselyaev, *Physical Review C* **75**, 054318 (2007).
 - [37] V. Soloviev, *Theory of Atomic Nuclei: Quasiparticles and Phonons* (Institute of Physics Publishing, 1992).
 - [38] L. A. Malov and V. G. Soloviev, *Nuclear Physics A* **270**, 87 (1976).
 - [39] V. I. Tselyaev, *Physical Review C* **88**, 054301 (2013).
 - [40] E. Litvinova, P. Ring, and V. Tselyaev, *Physical Review C* **75**, 064308 (2007).
 - [41] E. Litvinova, P. Ring, and V. Tselyaev, *Physical Review C* **78**, 014312 (2008).

- [42] E. Litvinova, P. Ring, and V. Tselyaev, *Physical Review Letters* **105**, 022502 (2010).
- [43] E. Litvinova, P. Ring, and V. Tselyaev, *Physical Review C* **88**, 044320 (2013).
- [44] V. Tselyaev, N. Lyutorovich, J. Speth, and P. G. Reinhard, *Physical Review C* **97**, 044308 (2018).
- [45] E. Litvinova, *Physical Review C* **107**, L041302 (2023).
- [46] E. Litvinova and Y. Zhang, *Physical Review C* **104**, 044303 (2021).
- [47] V. Van der Sluys, D. Van Neck, M. Waroquier, and J. Ryckebusch, *Nuclear Physics A* **551**, 210 (1993).
- [48] A. V. Avdeenkov and S. P. Kamerdzhiev, *Physics Letters B* **459**, 423 (1999).
- [49] A. V. Avdeenkov and S. P. Kamerdzhiev, *JETP Letters* **69**, 715 (1999).
- [50] F. Barranco, R. Broglia, G. Gori, E. Vigezzi, P. Bortignon, and J. Terasaki, *Physical Review Letters* **83**, 2147 (1999).
- [51] F. Barranco, P. Bortignon, R. Broglia, G. Colò, P. Schuck, E. Vigezzi, and X. Vinas, *Physical Review C* **72**, 054314 (2005).
- [52] V. I. Tselyaev, *Physical Review C* **75**, 024306 (2007).
- [53] E. V. Litvinova and A. V. Afanasjev, *Physical Review C* **84**, 014305 (2011).
- [54] E. Litvinova, *Physical Review C* **85**, 021303 (2012).
- [55] A. V. Afanasjev and E. Litvinova, *Physical Review C* **92**, 044317 (2015).
- [56] A. Idini, G. Potel, F. Barranco, E. Vigezzi, and R. A. Broglia, *Physical Review C* **92**, 031304 (2015).
- [57] V. Soma, T. Duguet, and C. Barbieri, *Physical Review C* **84**, 064317 (2011).
- [58] V. Soma, C. Barbieri, and T. Duguet, *Physical Review C* **87**, 011303 (2013).
- [59] V. Soma, C. Barbieri, and T. Duguet, *Physical Review C* **89**, 024323 (2014).
- [60] V. Somà, C. Barbieri, T. Duguet, and P. Navrátil, *European Physical Journal A* **57**, 135 (2021).
- [61] E. Litvinova and Y. Zhang, *Physical Review C* **106**, 064316 (2022).
- [62] D. R. Bes, R. A. Broglia, G. G. Dussel, and R. Liotta, *Physics Letters B* **56**, 109 (1975).
- [63] D. Bes, R. Broglia, G. Dussel, R. Liotta, and R. Prazzo, *Nuclear Physics A* **260**, 77 (1976).
- [64] J. Terasaki, F. Barranco, P. F. Bortignon, R. A. Broglia, and E. Vigezzi, *Progress in Theoretical Physics* **108**, 495 (2002).
- [65] Y. Niu, G. Colò, and E. Vigezzi, *Physical Review C* **90**, 054328 (2014).
- [66] Y. Niu, Z. Niu, G. Colò, and E. Vigezzi, *Physical Review Letters* **114**, 142501 (2015).
- [67] Y. F. Niu, G. Colo, E. Vigezzi, C. L. Bai, and H. Sagawa, *Physical Review C* **94**, 064328 (2016).
- [68] D. Gambacurta, M. Grasso, and F. Catara, *Physical Review C* **84**, 034301 (2011).
- [69] D. Gambacurta, M. Grasso, and J. Engel, *Physical Review C* **92**, 034303 (2015).
- [70] C. Robin and E. Litvinova, *European Physical Journal A* **52**, 205 (2016).
- [71] C. Robin and E. Litvinova, *Physical Review Letters* **123**, 202501 (2019).
- [72] V. Soloviev, C. Stoyanov, and A. Vdovin, *Nuclear Physics A* **288**, 376 (1977).
- [73] V. Yu. Ponomarev, P. F. Bortignon, R. A. Broglia, and V. V. Voronov, *Nuclear Physics A* **687**, 170 (2001).
- [74] F. Andreati, F. Knapp, N. Lo Iudice, A. Porrino, and J. Kvasil, *Physical Review C* **78**, 054308 (2008).
- [75] F. Knapp, N. Lo Iudice, P. Veselý, F. Andreati, G. De Gregorio, and A. Porrino, *Physical Review C* **90**, 014310 (2014).
- [76] S. Bacca, *Phys. Rev. C* **90**, 064619 (2014).
- [77] F. Knapp, N. Lo Iudice, P. Veselý, F. Andreati, G. De Gregorio, and A. Porrino, *Physical Review C* **92**, 054315 (2015).
- [78] G. De Gregorio, F. Knapp, N. Lo Iudice, and P. Vesely, *Physical Review C* **94**, 061301(R) (2016).
- [79] G. De Gregorio, F. Knapp, N. Lo Iudice, and P. Vesely, *Physical Review C* **93**, 044314 (2016).
- [80] V. Yu. Ponomarev, *Nucl. Phys.* **A649**, 243 (1999).
- [81] N. Lo Iudice, V. Y. Ponomarev, C. Stoyanov, A. V. Sushkov, and V. V. Voronov, *Journal of Physics G* **39**, 043101 (2012).
- [82] D. Savran *et al.*, *Phys. Rev.* **C84**, 024326 (2011).
- [83] N. Tsoneva, M. Spieker, H. Lenske, and A. Zilges, *Nuclear Physics A* **990**, 183 (2019).
- [84] H. Lenske and N. Tsoneva, *European Physical Journal A* **55**, 238 (2019).
- [85] M. Müscher *et al.*, *Physical Review C* **109**, 044318 (2024).
- [86] J. Novak, M. Q. Hlatshwayo, and E. Litvinova, (2024), arXiv:2405.02255 [nucl-th].
- [87] R. Brockmann, *Physical Review C* **18**, 1510 (1978).
- [88] A. Boyussy, J.-F. Mathiot, N. V. Giai, and S. Marcos, *Physical Review C* **36**, 380 (1987).
- [89] P. Poschenrieder and M. K. Weigel, *Physics Letters B* **200**, 231 (1988).
- [90] P. Poschenrieder and M. K. Weigel, *Physical Review C* **38**, 471 (1988).
- [91] P. Danielewicz and J. M. Namyslowski, *Physics Letters B* **81**, 110 (1979).
- [92] V. A. Karmanov, *Few Body Systems* **50**, 61 (2011).
- [93] G. Källén, *Helvetica Physica Acta* **25**, 417 (1952).
- [94] H. Lehmann, *Nuovo Cimento* **11**, 342 (1954).
- [95] P. Schuck, *Zeitschrift für Physik A* **279**, 31 (1976).
- [96] W. H. Dickhoff and C. Barbieri, *Progress in Particle and Nuclear Physics* **52**, 377 (2004).
- [97] W. H. Dickhoff and D. V. Neck, *Many-Body Theory Exposed!* (World Scientific, 2005).
- [98] H. Kucharek and P. Ring, *Zeitschrift für Physik A* **339**, 23 (1991).
- [99] N. Vinh Mau, in *Theory of nuclear structure, Trieste Lectures 1069*, p. 931 (IAEA, Vienna, 1970).
- [100] N. V. Mau and A. Bouyssy, *Nuclear Physics A* **257**, 189 (1976).
- [101] P. Ring and P. Schuck, *The Nuclear Many-Body Problem* (Springer-Verlag Berlin Heidelberg, 1980).
- [102] G. A. Rijsdijk, K. Allaart, and W. H. Dickhoff, *Nucl. Phys. A* **550**, 159 (1992).
- [103] C. Barbieri and M. Hjorth-Jensen, *Physical Review C* **79**, 064313 (2009).
- [104] C. Barbieri, *Physical Review Letters* **103**, 202502 (2009).
- [105] E. Litvinova and P. Ring, *Physical Review C* **73**, 044328 (2006).
- [106] P. Schuck, F. Villars, and P. Ring, *Nuclear Physics A* **208**, 302 (1973).
- [107] G. A. Rijsdijk, W. J. W. Geurts, K. Allaart, and W. H. Dickhoff, *Physical Review C* **53**, 201 (1996).
- [108] N. Bogolubov, *Journal of Physics* **11**, 23 (1947).

- [109] Y. Zhang, A. Bjelčić, T. Nikšić, E. Litvinova, P. Ring, and P. Schuck, *Physical Review C* **105**, 044326 (2022).
- [110] G. A. Lalazissis, J. König, and P. Ring, *Physical Review C* **55**, 540 (1997).
- [111] G. A. Lalazissis, S. Karatzikos, R. Fossion, D. P. Arteaga, A. V. Afanasjev, and P. Ring, *Physics Letters B* **671**, 36 (2009).
- [112] D. Vretenar, A. V. Afanasjev, G. A. Lalazissis, and P. Ring, *Physics Reports* **409**, 101 (2005).
- [113] P. Avogadro and T. Nakatsukasa, *Physical Review C* **84**, 014314 (2011).
- [114] P. Schuck and M. Tohyama, *Physical Review B* **93**, 165117 (2016).
- [115] V. Zelevinsky and A. Volya, *Physics of Atomic Nuclei* (Wiley, 2017).
- [116] N. Lyutorovich, V. Tselyaev, J. Speth, and P. Reinhard, *Physical Review C* **98**, 054304 (2018).
- [117] Y. Niu, Z. Niu, G. Colò, and E. Vigezzi, *Physics Letters B* **780**, 325 (2018).
- [118] E. Litvinova, H. Loens, K. Langanke, G. Martinez-Pinedo, T. Rauscher, P. Ring, F.-K. Thielemann, and V. Tselyaev, *Nuclear Physics A* **823**, 26 (2009).
- [119] J. Endres, E. Litvinova, D. Savran, P. A. Butler, M. N. Harakeh, S. Harissopulos, R.-D. Herzberg, R. Krücken, A. Lagoyannis, N. Pietralla, V. Y. Ponomarev, L. Popescu, P. Ring, M. Scheck, K. Sonnabend, V. I. Stoica, H. J. Wörtche, and A. Zilges, *Physical Review Letters* **105**, 212503 (2010).
- [120] R. Massarczyk, R. Schwengner, F. Dönau, E. Litvinova, G. Rusev, R. Beyer, R. Hannaske, A. Junghans, M. Kempe, J. H. Kelley, *et al.*, *Physical Review C* **86**, 014319 (2012).
- [121] E. Lanza, A. Vitturi, E. Litvinova, and D. Savran, *Physical Review C* **89**, 041601 (2014).
- [122] I. Poltoratska, R. Fearick, A. Krumbholz, E. Litvinova, H. Matsubara, P. von Neumann-Cosel, V. Y. Ponomarev, A. Richter, and A. Tamii, *Physical Review C* **89**, 054322 (2014).
- [123] D. Negi, M. Wiedeking, E. G. Lanza, E. Litvinova, A. Vitturi, R. A. Bark, L. A. Bernstein, D. L. Bleuel, D. S. Bvumbi, T. D. Bucher, B. H. Daub, T. S. Dinoko, N. Erasmus, J. L. Easton, A. Görden, M. Guttormsen, P. Jones, B. V. Kheswa, N. Khumalo, A. C. Larsen, E. A. Lawrie, J. J. Lawrie, S. N. T. Majola, L. P. Masiteng, M. R. Nchodu, J. Ndayishimye, R. T. Newman, S. P. Noncolela, J. N. Orce, P. Papka, T. Renstrøm, D. G. Roux, O. Shirinda, S. Siem, P. S. Sithole, and P. C. Uwitonze, *Physical Review C* **94**, 024332 (2016).
- [124] I. A. Egorova and E. Litvinova, *Physical Review C* **94**, 034322 (2016).
- [125] J. Carter *et al.*, *Physics Letters B* **833**, 137374 (2022).
- [126] M. Scott *et al.*, *Physical Review Letters* **118**, 172501 (2017).
- [127] C. Robin and E. Litvinova, *Physical Review C* **98**, 051301(R) (2018).
- [128] E. Litvinova and H. Wibowo, *Physical Review Letters* **121**, 082501 (2018).
- [129] E. Litvinova and H. Wibowo, *European Physical Journal A* **55**, 223 (2019).
- [130] E. Litvinova, C. Robin, and H. Wibowo, *Physics Letters B* **800**, 135134 (2020).
- [131] E. Litvinova and C. Robin, *Physical Review C* **103**, 024326 (2021).
- [132] B. S. Ishkhanov and I. M. Kapitonov, *Phys.-Uspekhi* **64**, 141 (2021).
- [133] M. N. Harakeh and A. can der Woude, *Giant Resonances: Fundamental High-Frequency Modes of Nuclear Excitation* (Oxford University Press, 2001).
- [134] D. Savran, T. Aumann, and A. Zilges, *Progress in Particle and Nuclear Physics* **70**, 210 (2013).
- [135] U. Garg and G. Colò, *Prog. Part. Nucl. Phys.* **101**, 55 (2018).
- [136] V. Tselyaev, N. Lyutorovich, J. Speth, and P. G. Reinhard, *Phys. Rev. C* **102**, 064319 (2020).
- [137] G. E. Brown and M. Bolsterli, *Physical Review Letters* **3**, 472 (1959).
- [138] R. Broglia and V. Zelevinsky, eds., *Fifty Years Of Nuclear BCS: Pairing In Finite Systems* (World Scientific, 2013).
- [139] J. Meng, ed., *Relativistic Density Functional for Nuclear Structure*, International Review of Nuclear Physics, Vol. 10 (World Scientific, Singapore, 2016).
- [140] N. Paar, P. Ring, T. Nikšić, and D. Vretenar, *Physical Review C* **67**, 034312 (2003).
- [141] National Nuclear Data Center, <https://www.nndc.bnl.gov>.
- [142] J. Meng, H. Toki, S. G. Zhou, S. Q. Zhang, W. H. Long, and L. S. Geng, *Progress in Particle and Nuclear Physics* **57**, 470 (2006).
- [143] L. Trippa, G. Colo, and E. Vigezzi, *Physical Review C* **77**, 061304 (2008), arXiv:0802.3658 [nucl-th].
- [144] P. Papakonstantinou and R. Roth, *Phys. Lett. B* **671**, 356 (2009).
- [145] S. Shlomo and G. Bertsch, *Nuclear Physics A* **243**, 507 (1975).
- [146] V. Tselyaev, N. Lyutorovich, J. Speth, S. Krewald, and P. G. Reinhard, *Physical Review C* **94**, 034306 (2016).
- [147] S. Kamerdzhiev, R. J. Liotta, E. Litvinova, and V. Tselyaev, *Physical Review C* **58**, 172 (1998).
- [148] K. Hagino and H. Sagawa, *Nuclear Physics A* **695**, 82 (2001).
- [149] M. Matsuo, *Progress of Theoretical Physics Supplement* **146**, 110 (2002).
- [150] E. Khan, N. Sandulescu, M. Grasso, and N. Van Giai, *Physical Review C* **66**, 024309 (2002).
- [151] J. Daoutidis, *Physical Review C* **80**, 024309 (2009).
- [152] D. M. Rossi, P. Adrich, F. Aksouh, H. Alvarez-Pol, T. Aumann, J. Benlliure, M. Böhmer, K. Boretzky, E. Casarejos, M. Chartier, A. Chatillon, D. Cortina-Gil, U. Datta Pramanik, H. Emling, O. Ershova, B. Fernandez-Dominguez, H. Geissel, M. Gorska, M. Heil, H. T. Johansson, A. Junghans, A. Kelic-Heil, O. Kiselev, A. Klimkiewicz, J. V. Kratz, R. Krücken, N. Kurz, M. Labiche, T. Le Bleis, R. Lemmon, Y. A. Litvinov, K. Mahata, P. Maierbeck, A. Movsesyan, T. Nilsson, C. Nociforo, R. Palit, S. Paschalis, R. Plag, R. Reifarth, D. Savran, H. Scheit, H. Simon, K. Sümmerer, A. Wagner, W. Waluś, H. Weick, and M. Winkler, *Physical Review Letters* **111**, 242503 (2013).
- [153] E. Litvinova, *Physical Review C* **91**, 034332 (2015).
- [154] D. P. Arteaga and P. Ring, *Physical Review C* **77**, 034317 (2008).
- [155] S. Peru and H. Goutte, *Physical Review C* **77**, 044313 (2008).
- [156] J. Toivanen, B. G. Carlsson, J. Dobaczewski, K. Mizuyama, R. R. Rodriguez-Guzman, P. Toivanen,

- and P. Vesely, *Physical Review C* **81**, 034312 (2010).
- [157] T. Nakatsukasa, T. Inakura, and K. Yabana, *Physical Review C* **76**, 024318 (2007).
- [158] T. Oishi, M. Kortelainen, and N. Hinohara, *Physical Review C* **93**, 034329 (2016).
- [159] T. Nikšić, N. Kralj, T. Tutiš, D. Vretenar, and P. Ring, *Physical Review C* **88**, 044327 (2013).
- [160] M. Kortelainen, N. Hinohara, and W. Nazarewicz, *Physical Review C* **92**, 051302 (2015).
- [161] Q. Liu, J. Engel, N. Hinohara, and M. Kortelainen, *Physical Review C* **109**, 044308 (2024).
- [162] F. Osterfeld, *Review of Modern Physics* **64**, 491 (1992).
- [163] M. Ichimura, H. Sakai, and T. Wakasa, *Progress in Particle and Nuclear Physics* **56**, 446 (2006).
- [164] N. Paar, D. Vretenar, E. Khan, and G. Coló, *Rep. Prog. Phys.* **70**, 691 (2007).
- [165] X. Roca-Maza and N. Paar, *Progress in Particle and Nuclear Physics* **101**, 96 (2018).
- [166] A. Krasznahorkay, M. Fujiwara, P. van Aarle, H. Akimune, I. Daito, H. Fujimura, Y. Fujita, M. N. Harakeh, T. Inomata, J. Jänecke, S. Nakayama, A. Tamii, M. Tanaka, H. Toyokawa, W. Uijen, and M. Yosoi, *Physical Review Letters* **82**, 3216 (1999).
- [167] K. Yako, H. Sagawa, and H. Sakai, *Physical Review C* **74**, 051303(R) (2006).
- [168] X. Roca-Maza, G. Colo, and H. Sagawa, *Physical Review C* **86**, 031306 (2012).
- [169] H. Liang, N. Van Giai, and J. Meng, *Physical Review Letters* **101**, 122502 (2008).
- [170] Z. M. Niu, Y. F. Niu, H. Z. Liang, W. H. Long, T. Nikšić, D. Vretenar, and J. Meng, *Physics Letters B* **723**, 172 (2013).
- [171] Z. M. Niu, Y. F. Niu, H. Z. Liang, W. H. Long, and J. Meng, *Physical Review C* **95**, 044301 (2017).
- [172] I. N. Borzov, *Physical Review C* **67**, 025802 (2003).
- [173] P. Sarriguren, *Physical Review C* **87**, 045801 (2013).
- [174] N. Paar, T. Nikšić, D. Vretenar, and P. Ring, *Physical Review C* **69**, 054303 (2004).
- [175] S. Drozdz, S. Nishizaki, J. Speth, and J. Wambach, *Physics Reports* **197**, 1 (1990).
- [176] T. Marketin, E. Litvinova, D. Vretenar, and P. Ring, *Physics Letters B* **706**, 477 (2012).
- [177] D. Gambacurta, M. Grasso, and J. Engel, *Physical Review Letters* **125**, 212501 (2020).
- [178] E. Litvinova, B. Brown, D.-L. Fang, T. Marketin, and R. Zegers, *Physics Letters B* **730**, 307 (2014).
- [179] K. Yako *et al.*, *Physics Letters B* **615**, 193 (2005).
- [180] T. Wakasa *et al.*, *Physical Review C* **55**, 2909 (1997).
- [181] S. P. Kamerdzhiev, G. Y. Tertychny, and V. I. Tselyaev, *Physics of Particles and Nuclei* **28**, 134 (1997).
- [182] J. Terasaki, *Physical Review C* **97**, 034304 (2018).
- [183] T. Kajino, W. Aoki, A. Balantekin, R. Diehl, M. Famiano, and G. Mathews, *Progress in Particle and Nuclear Physics* **107**, 109 (2019).
- [184] E. Litvinova, P. Ring, V. Tselyaev, and K. Langanke, *Physical Review C* **79**, 054312 (2009).
- [185] T. Nikšić, T. Marketin, D. Vretenar, N. Paar, and P. Ring, *Physical Review C* **71**, 014308 (2005), arXiv:nucl-th/0412028 [nucl-th].
- [186] M. T. Mustonen and J. Engel, *Phys. Rev. C* **93**, 014304 (2016).
- [187] A. A. Dzhiyev, K. Langanke, G. Martínez-Pinedo, A. I. Vdovin, and C. Stoyanov, *Physical Review C* **101**, 025805 (2020).
- [188] M. Arnould, S. Goriely, and K. Takahashi, *Phys. Rep.* **450**, 97 (2007).
- [189] M. Mumpower, R. Surman, G. McLaughlin, and A. Aprahamian, *Progress in Particle and Nuclear Physics* **86**, 86 (2016).
- [190] K. Langanke, G. Martínez-Pinedo, and R. Zegers, *Reports on Progress in Physics* **84**, 066301 (2021).
- [191] J. J. Cowan, C. Sneden, J. E. Lawler, A. Aprahamian, M. Wiescher, K. Langanke, G. Martínez-Pinedo, and F.-K. Thielemann, *Reviews of Modern Physics* **93**, 15002 (2021).